Research Paper

Characterizing a long-term chronic heart failure model by transcriptomic alterations and monitoring of cardiac remodeling

Yingqi Zhu[1], Qiancheng Wang[1], Hairuo Lin[1], Kaitong Chen[1], Cankun Zheng[1], Lin Chen[1], Siyuan Ma[1], Wangjun Liao[3], Jianping Bin[1], Yulin Liao[1,2]

[1]Department of Cardiology, State Key Laboratory of Organ Failure Research, Guangdong Provincial Key Lab of Shock and Microcirculation, Nanfang Hospital, Southern Medical University, Guangzhou 510515, China
[2]Bioland Laboratory, Guangzhou Regenerative Medicine and Health Guangdong Laboratory, Guangzhou 510005, China
[3]Department of Oncology, Nanfang Hospital, Southern Medical University, Guangzhou 510515, China

Correspondence to: Yulin Liao, Qiancheng Wang; **email:** liao18@msn.com, https://orcid.org/0000-0001-5961-390X; wqc820802@smu.edu.cn
Keywords: transcriptomic profiling, myocardial infarction, heart failure, mice, cardiac remodeling
Received: July 8, 2020 **Accepted:** March 2, 2021 **Published:** April 23, 2021

ABSTRACT

The long-term characteristics of transcriptomic alterations and cardiac remodeling in chronic heart failure (CHF) induced by myocardial infarction (MI) in mice are not well elucidated. This study aimed to reveal the dynamic changes in the transcriptome and cardiac remodeling in post-MI mice over a long time period. Monitoring C57BL/6 mice with MI for 8 months showed that approximately 44% of mice died of cardiac rupture in the first 2 weeks and others survived to 8 months with left ventricular (LV) aneurysm. The transcriptomic profiling analysis of cardiac tissues showed that the Integrin and WNT pathways were activated at 8 months after MI while the metabolism-related pathways were inversely inhibited. Subsequent differential analysis at 1 and 8 months post-MI revealed significant enrichments in biological processes, including consistent regulation of metabolism-related pathways. Moreover, echocardiographic monitoring showed a progressive increase in LV dimensions and a decrease in the LV fractional shortening during the first 4 weeks, and these parameters progressed at a lower rate till 8 months. A similar trend was found in the invasive LV hemodynamics, cardiac morphological and histological analyses. These results suggested that mouse MI model is ideal for long-term studies, and transcriptomic findings may provide new CHF therapeutic targets.

INTRODUCTION

Chronic heart failure (CHF) induced by myocardial infarction (MI) causes high rates of hospitalization and mortality, which is a major health burden worldwide [1]. Patients with MI without timely coronary reperfusion would suffer chronic cardiac remodeling [2]. Despite strides forward in the treatment and management of MI [3, 4], the current therapies used to prevent or delay the progression of cardiac remodeling are limited. Thus, it is very necessary to use animal models of post-MI chronic cardiac remodeling to investigate and explore the pathophysiological and transcriptomic changes associated with advanced heart failure to identify new therapeutic targets. In the era of evidence-based medicine, long-term observation has increased in many clinical studies. Vallejo-Vaz *et al.* carried out a 20-year follow-up to evaluate the long-term benefits of lowering low-density lipoprotein cholesterol for the primary prevention of cardiovascular disease in patients enrolled in the WOSCOPS trial [5]. Twenty years of a human life span is comparable to approximately 8 months for mouse [6]. The mouse MI model is the most frequently used animal model for studies on post-MI remodeling, and this model is generally utilized with an observational period of 3–6 weeks [7, 8], However, the long-term (e.g., several

months) characteristics as well as transcriptomic level changes of this model have not been well elucidated. After an ischemic insult, the myocardium can exhibit distinct responses, leading to myocardial stunning, hibernation, or activation of cellular mechanisms. However, in long-time ischemic myocardium, structural cardiac remodeling leads to irreversible heart failure due to progressive fibrosis, metabolism pathway switching, and unique transcriptomic alterations [9]. To elucidate the pathogenesis of heart failure and identify novel therapeutic targets, it is important to better understand the molecular bases of the long-term ischemic and failing cardiomyocyte states as well as to identify regulators of the transition between states. Uncovering the gene programs involved in long-term ischemic cardiac dysfunction would enable accurate assessment of the cardiomyocyte condition and prediction of treatment response [10].

To date, studies have rarely addressed the distinct mRNA expression profiles in mice with long-term MI lasting for several months. Very little is known about the expression profile of mRNA transcript in the advanced failing heart. In this study, transcriptomic profiling analyses were performed on cardiac tissue using RNA sequencing (RNA-seq) technology in sham and 8 months post-MI mice. We performed Weighted Gene Co-expression Network Analysis (WGCNA), Gene Set Enrichment Analysis (GSEA) and Protein-Protein Interaction Network (PPI) to detect the characteristics of transcriptomic alterations of heart in advanced heart failure mice. More importantly, we used Principal Component Analysis (PCA) and Gene Ontology (GO) analysis to compare our sequencing data with open access datasets derived from cardiac tissue of 4 weeks post-MI mice (GSE96566; https://www.ncbi.nlm.nih.gov/geo/query/acc.cgi?acc=GSE96566) [11].

In addition to the distinct transcriptomic changes, we found that the electrocardiogram (ECG), echocardiography, invasive LV (left ventricle) hemodynamics, heart and lung histology, and molecular biomarkers also showed dynamic change during post-MI remodeling in an 8-month time period.

We present the following article/case in accordance with the animal research reporting checklist.

RESULTS

Confirmation of MI success

We generated a mouse MI model by ligation of the left coronary artery (LCA). Lead II ECG was used to monitor the evolution of ECG during the time course. As shown in Figure 1A, the ST segment with an upward roach back elevation immediately appeared in leads I, II and III when the LCA was tied, indicating the occurrence of myocardial ischemia and that the limb leads reflected the myocardial ischemia induced by LCA occlusion. Therefore, we employed lead II ECG to assess the correct ligature placement and monitor ECG changes in response to MI throughout the time course. The elevated ST segment started to fall after 30 minutes of MI (Figure 1B). One day after MI, the ST segment dropped to a baseline level, and the T wave became inverted to be recorded at day 3rd, this trend recovered during 1 month and then persisted to 8 months after MI (Figure 1B). A pathological Q wave appeared 1 day after MI and persisted to even 8 months as pointed out by the black arrows in Figure 1B. Acute infarct size was calculated from the TTC (Triphenyl tetrazolium chloride) staining of heart sections. As shown in Figure 1C, the brick-red staining indicated viable tissue, while the unstained white sections represented infarct area. Our approach showed similar infarct size (infarct area/LV area) with low dispersion among different mice (Figure 1C). In this model, the ventricular aneurysm was generally formed at one week after MI (Figure 1D). Most of the mice that survived after 2 months survived until as long as 8 months, but they exhibited decreased exercise tolerance and shortness of breath (Supplementary Figure 1 and Supplementary Video 1).

Survival rate over eight months

Kaplan–Meier survival analysis indicated that the total mortality was 42% for mice with MI and 0% for sham-operated mice during the 8 months of observation (Figure 1F). The first 2-week mortality rate after MI remained at approximately 40% when the sample size was enlarged from 40 to 117 (Figure 1G). Most deaths occurred in the first 10 days after MI due to cardiac rupture (Figure 1E). For the MI mice that survived to 4 weeks, the mortality afterward was very low, which may have been due to the individual differences in compensation reactivity and tolerances.

Identification of transcriptomic status in the hearts of mice with MI for 8 months

To date, studies have rarely addressed the distinct mRNA expression profiles in long-term MI models as long as 8 months. To obtain a comprehensive understanding of transcriptome alterations during the long term post-MI status of mice, RNA-seq measurements were performed on cardiac tissues in the sham group and 8-month MI group (Supplementary raw data).

We used the WGCNA package to construct co-expression modules for cluster analysis. Based on the

histological grade by average linkage clustering, 7 modules were identified and the green module, which contained 86 genes, had the highest significant correlation coefficient with the trait (Figure 2A). GO enrichment analysis was then performed using these 86 genes (Supplementary Table 1), and the results in Figure 2B shows that the genes related to RNA Polymerase-1 mediated biological processes were

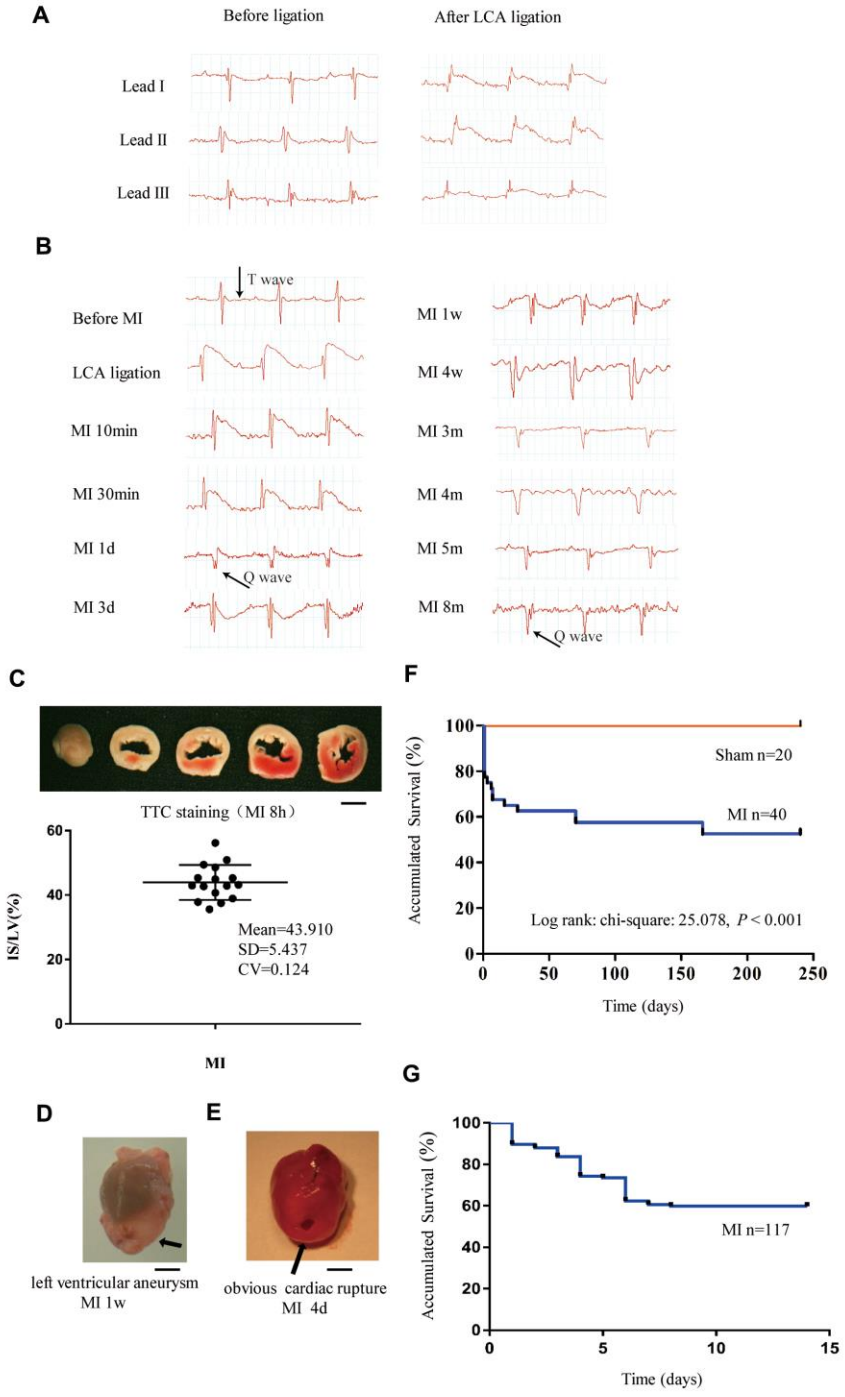

Figure 1. Monitoring of long-term MI mouse model for 8 months. (**A**) Limb leads I, II and III of electrocardiogram (ECG) reliably reflect the acute ischemia induced by left coronary ligation in C57BL/6 mice. (**B**) Lead II ECG can reflect different stages of myocardial infarction (MI) for a time period of 8 months. (**C**) Triphenyl tetrazolium chloride (TTC)-stained sections of heart in mice with MI for 8 h; the infarct size (IS)/ left ventricle (LV) was approximately 44% in the MI groups. (**D**) Representative left ventricular aneurysm formed 1 week after MI; (**E**) Example necropsy images of a dead mouse showing obvious rupture in the left ventricle free wall. (**F**): Kaplan–Meier survival analysis of mice subjected to MI or sham operation for 8 months. (**G**) Kaplan–Meier survival analysis of mice subjected to MI or sham operation for 14 days, *n* = 114 in MI group; Scale bar =2 mm for panel (**C, D** and **E**).

significantly upregulated. To further elucidate the potential mechanisms of gene alterations in 8 months post-MI regulation, we performed GSEA analysis and a total of 3398 genes were detected in the profiling. All the genes were grouped into 893 gene sets. According to the gene set size filters (min = 15, max = 500), 771 gene sets were filtered out and the remaining 122 gene sets were used in the analysis. The GSEA analysis

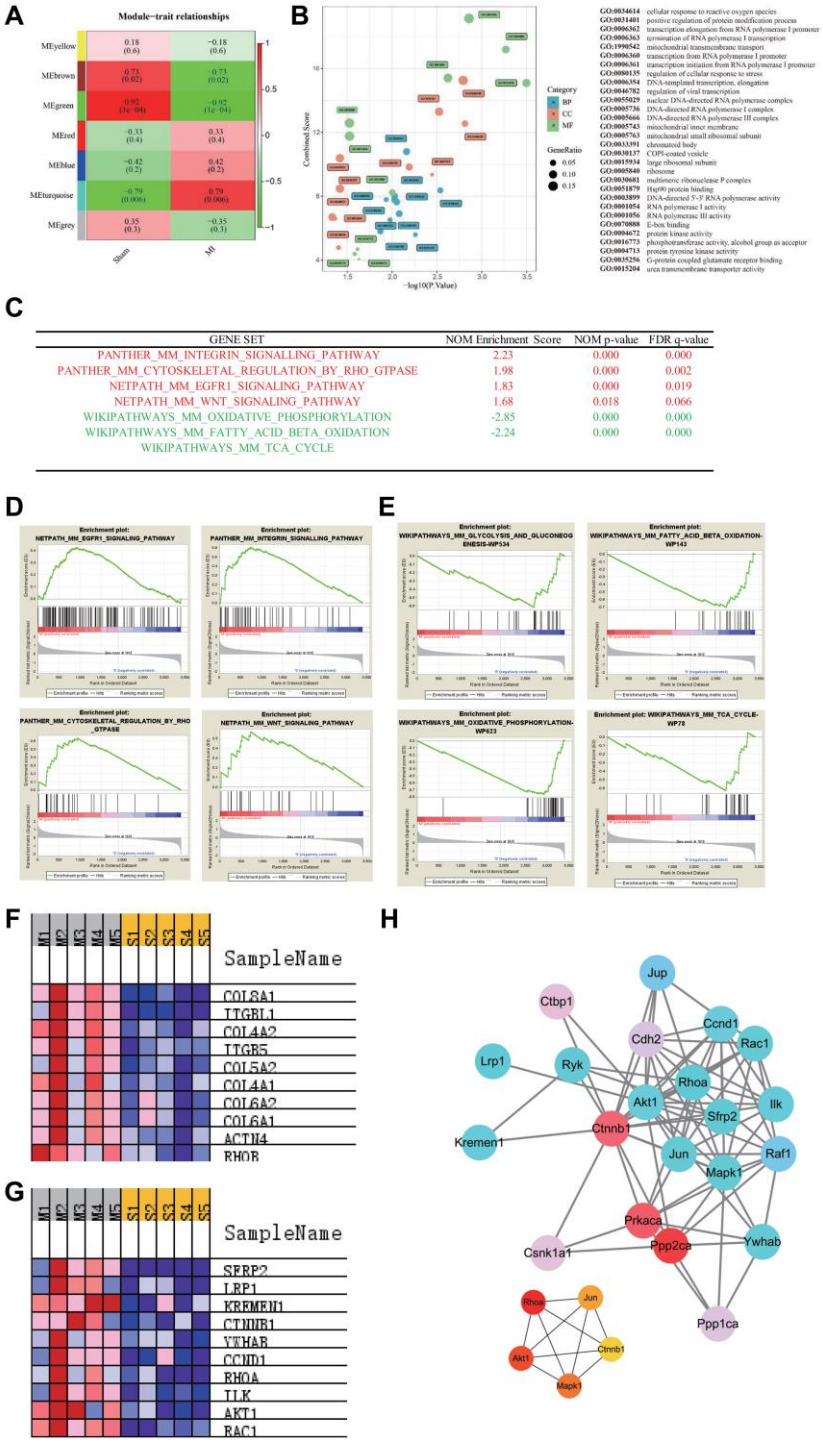

Figure 2. Pathways enrichment associated with advanced heart failure. (**A**) WGCNA identified demonstrated 7 modules by average linkage clustering. (**B**) Gene Ontology analysis of genes in the green module, which were more correlated with advanced heart failure. (**C**) List of the four significantly up-regulated (marked red) and four down-regulated gene sets (marked green) associated with advanced heart failure enriched in GSEA analysis. (**D**–**E**) Enrichment plots of four significantly up-regulated and down-regulated pathways. (**F**) Heatmap of the enriched genes in the Integrin signaling pathway. (**G**) Heatmap of the enriched genes in the WNT signaling pathway. (**H**) Protein-protein interaction network of WNT signaling pathway and hub genes involved in this network.

showed that 9 gene sets were significantly enriched at *P* value < 0.01 in the MI group (Supplementary Table 2), while 6 gene sets were significantly enriched in the sham group (Supplementary Table 3). Gene sets enrichments revealed that the Integrin and WNT pathways were activated and that the metabolism-related pathways (fatty acid beta oxidation, glycolysis and TCA cycle pathways) were inversely inhibited 8 months after MI (Figure 2C–2E and Supplementary Figure 2). In addition, the expression of the top 10 genes involved in the abovementioned pathways are shown in Figure 2F–2G and Supplementary Tables 4–8. We then screened the WNT signaling pathway-related genes that were significantly up-regulated in the GSEA analysis. The top four contributing genes in this pathway were SFRP2, LRP1, KREMEN1, CTNNB1. We next used the String database to analyze PPI. MCC selection of the top ranked nodes in the network demonstrated that CTNNB1 was located at the core of the network, indicating that CTNNB1 is the hub gene (Figure 2H). Thus, these findings suggested that CTNNB1 should play an important role in the transcriptome regulation of long-term MI.

Alterations of molecular signature from 1 month to 8 months after MI

Global clustering of the transcriptomic profiles of mice at 1 month and 8 months after MI was performed. PCA with arbitrary parameters was used to identify the differentially expressed genes in the different status through the distribution position. The results indicated that there was a large difference in gene expression between the two time points of MI (Figure 3A and Supplementary raw data). Differential analysis demonstrated that 303 and 384 genes were differentially regulated at 1 month and 8 month post MI respectively, according to the threshold of padj (adjust *P* value) <0.05 and that 95 genes were simultaneously differentially regulated at both time points (Figure 3B and Supplementary Table 9). Most genes showed a continuous alteration trend at both time points, but some genes, including Kif2c, Pira2 and Rassf10, showed an inverted trend (marked by red in Supplementary Table 9). Enrich Gene Ontology (EGO) and Group Gene Ontology (GGO) analysis revealed that metabolism related pathways persisted throughout the time course. EGO analysis revealed more independent differences than GGO, including the enrichment of axonogenesis related biological processes at 1 month as well as sensory organ morphogenesis and cell division regulation at 8 months (Figure 3C). With regard to the common altered biological processes in EGO analysis, the urogenital and renal system development made the greatest contribution (Figure 3C).

Verifying time-course changes of echocardiography

M-mode echocardiography was used to evaluate the cardiac remodeling and verify heart function alteration (Figure 4A). We found a progressive increase in left ventricular end-systolic (LVESd) and end-diastolic diameters (LVEDd) as well as a progressive decrease in the left ventricular ejection fraction (LVEF) and fractional shortening (LVFS) during the first 4 weeks after MI compared to the sham group (Figure 4B–4E). Four weeks later, those parameters were maintained at relatively stable levels.

LV hemodynamic characterization in long term post-MI model

To characterize the long term post-MI cardiac efficiency alterations, the LV hemodynamics in MI or sham mice were measured at 4 time points (Figure 5A). Compared with that in the sham mice, the systolic pressure (LVSP) was decreased and end diastolic pressure (LVEDP) was significantly increased in MI mice. Moreover, the LV pressures were stable at 1 week, 4 weeks, and 8 months after MI (Figure 5B–5C). A time-dependent reduction of systolic function was evidenced by a progressive decrease in the maximum rates of change in the LV pressure (*dP/dt max*) and LV contractility in MI mice (Figure 5D–5F). After MI, *dP/dt min* was significantly decreased and persisted to 8 months, while the exponential time constant of relaxation (τ) was progressively extended (Figure 5E–5G), indicating a dysfunction of diastolic function.

Characterizing morphological remodeling

Consistent with the molecular changes, a time-dependent enlargement of cardiac cavity after MI was observed (Figure 6A and Supplementary Figure 3). At 1 week to 8 months after MI, both the heart weight/body weight ratio and heart weight/tibia length ratio were significantly higher than in the sham group, and both ratios were even higher at 8-months after MI (Figure 6B–6C). Moreover, the heart weight/tibia length ratio at 8 months after MI was significantly higher than that at 4 weeks post-MI (Figure 6C). The lung weight/body weight ratio and the lung weight/tibia length ratio were significantly higher at the 3 indicated time points in the post-MI group than the corresponding time points in the sham group (Figure 6D–6E), and the lung weight/tibia length ratio was higher at 4 weeks and 8 months post MI than at 1 week post-MI (Figure 6D–6E), a liver congestion indicated by larger LiW/BW and LiW/TL was also observed (Supplementary Figure 4A and 4B). We next performed real-time PCR analysis to verify the biomarkers of heart failure in MI mice at the indicated time points based on the transcriptomic analysis (Figure 6F–6H). Both the ANP and β-MHC genes were significantly upregulated at 4 weeks and 8 months after MI (Figure 6F and 6H). In

accordance with the GSEA analysis, the gene expression of α-MHC was not significantly changed (Figure 6G), and the expression levels of ANP and β-MHC were much higher at 8 months post-MI than 4 weeks post-MI (Figure 6F and 6H).

DISCUSSION

In the present study, we characterized a long-term mouse model of heart failure. The following observations were made: (1) Limb lead II ECG is sufficient to reflect the

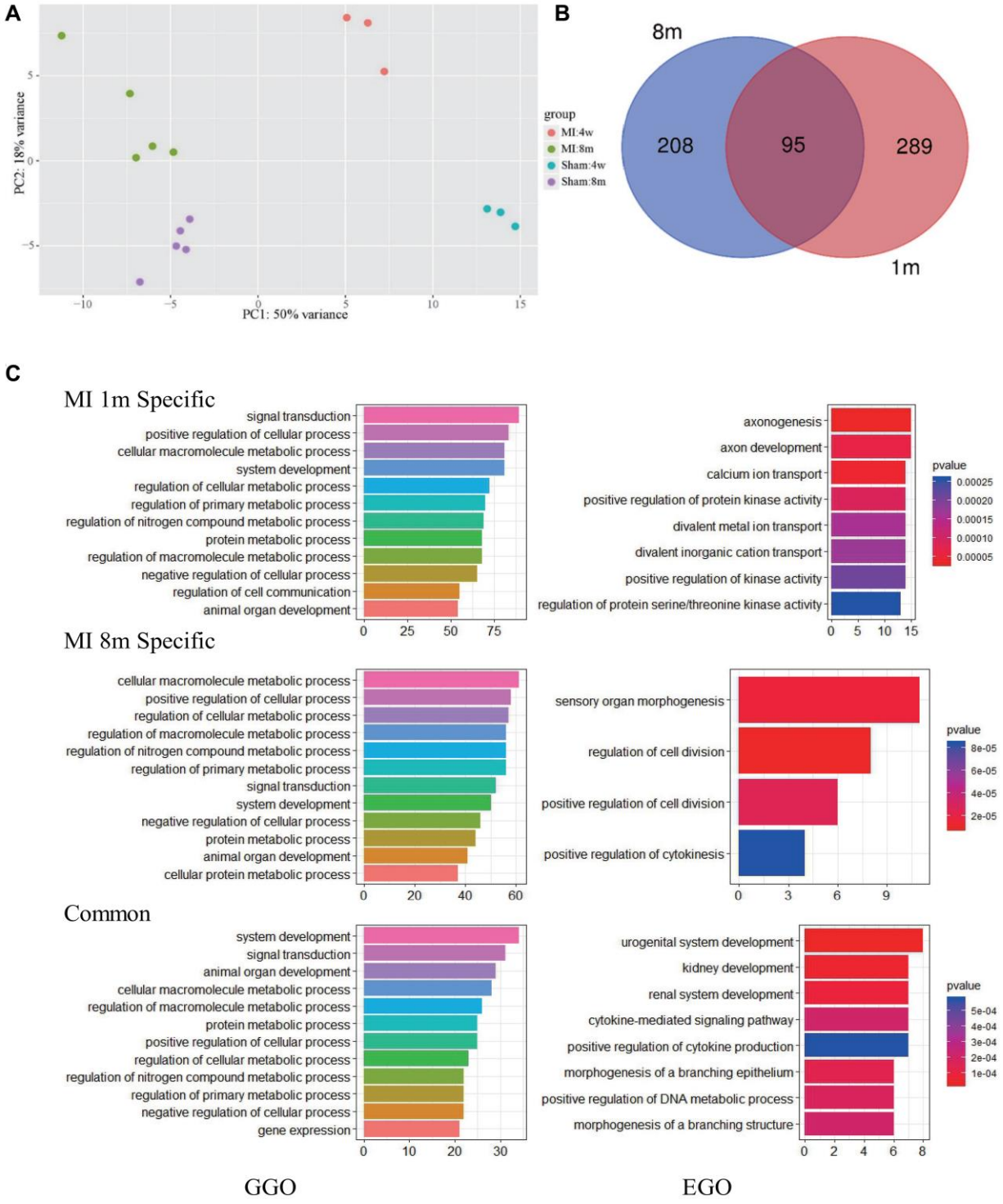

Figure 3. Pathways most affected at 1 month and 8 months after MI. (**A**) PCA analysis show that the transcriptome of mice after LCA ligation changes significantly and varies with time. (**B**) Overlap of significantly modulated genes between 1 month and 8 months post-MI. (**C**) GGO (left) and EGO (right) analysis of pathways affected by long term MI.

phases of MI such as acute ischemia and old MI; (2) Most mice that survive to 4 weeks after MI can survive to as long as 8 months; (3) We first summarized the genetic alterations at 8 months after MI by WGCNA and GSEA. PCA and GO analysis suggested that the transcriptomic profiles are different at 1 month and 8 months after MI. (4) Echocardiography, invasive measurement of LV hemodynamic, histological examinations and molecular examinations successfully verified the predicted changes in molecular pathways and characterized this long-term chronic heart failure mouse model. Therefore, this long-term MI model is suitable as a chronic heart failure model to investigate the long term effects of various therapeutic approaches, which would be much more clinically relevant.

The MI mouse model has been frequently used to elucidate the mechanisms involved in myocardial injury

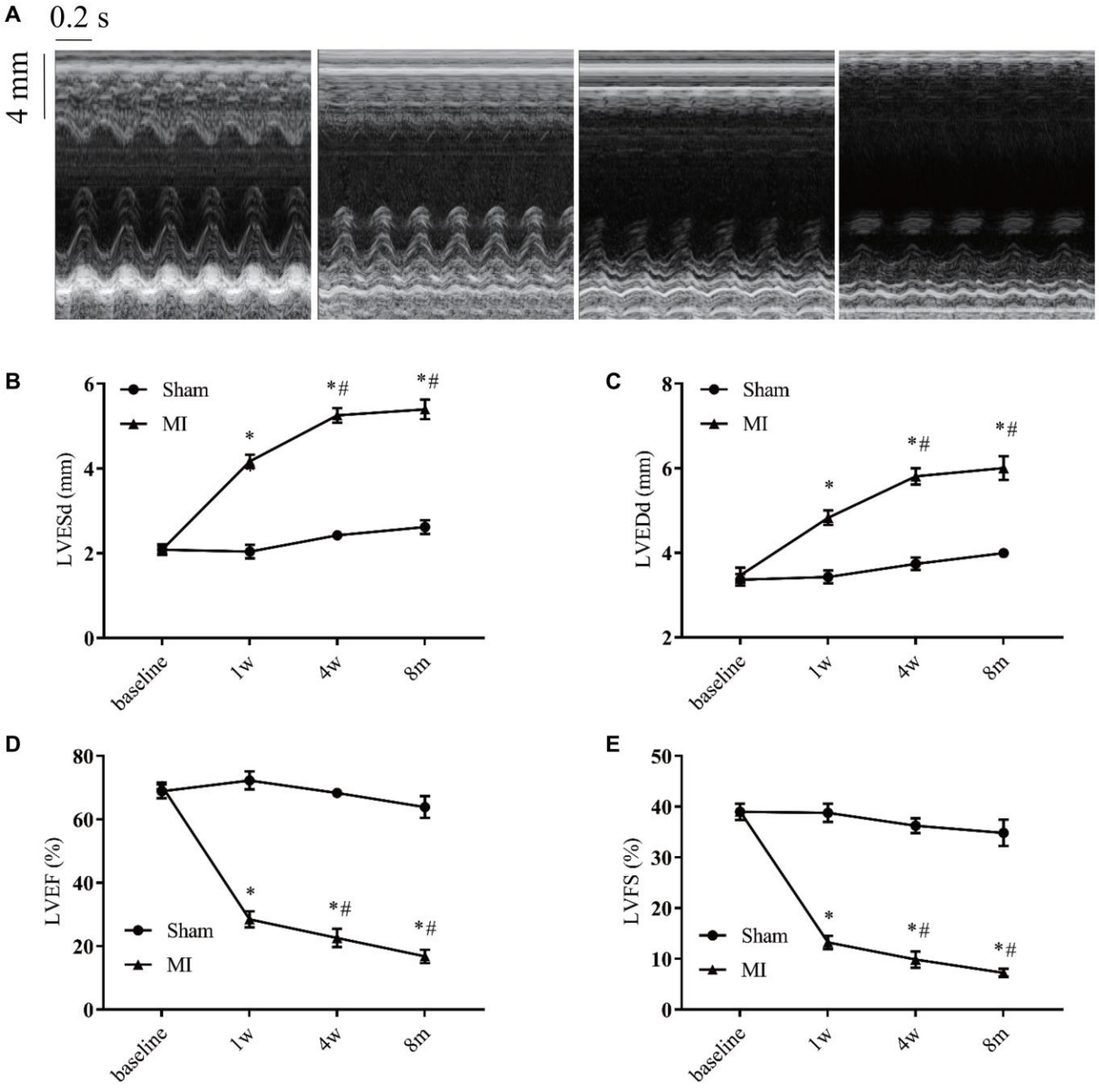

Figure 4. Serial echocardiographic assessment of post-infarction remodeling. (**A**) Representative recordings of M-mode echocardiographic images at indicated time points. (**B**) Left ventricular end-systolic diameter (LVESd). (**C**) Left ventricular end-diastolic diameter (LVEDd). (**D**) Left ventricular systolic function presented by the left ventricular ejection fraction (LVEF). (**E**) Left ventricle fractional shortening (LVFS). $^{*}P < 0.05$ vs the corresponding time point in the sham group. $^{\#}P < 0.05$ compared with the prior time point in the MI group. n = 8–10 at various time points.

and cardiac remodeling and to investigate the effects of therapeutic interventions at preclinical stages. Conventional treatments for post-MI heart failure can partly delay cardiac remodeling, improve quality of life, and reduce risk of heart failure-related hospitalization and death [12, 13]. However, the 5-year mortality rate of heart failure remains as high as approximately 50%. Thus, it is necessary to identify new therapeutic

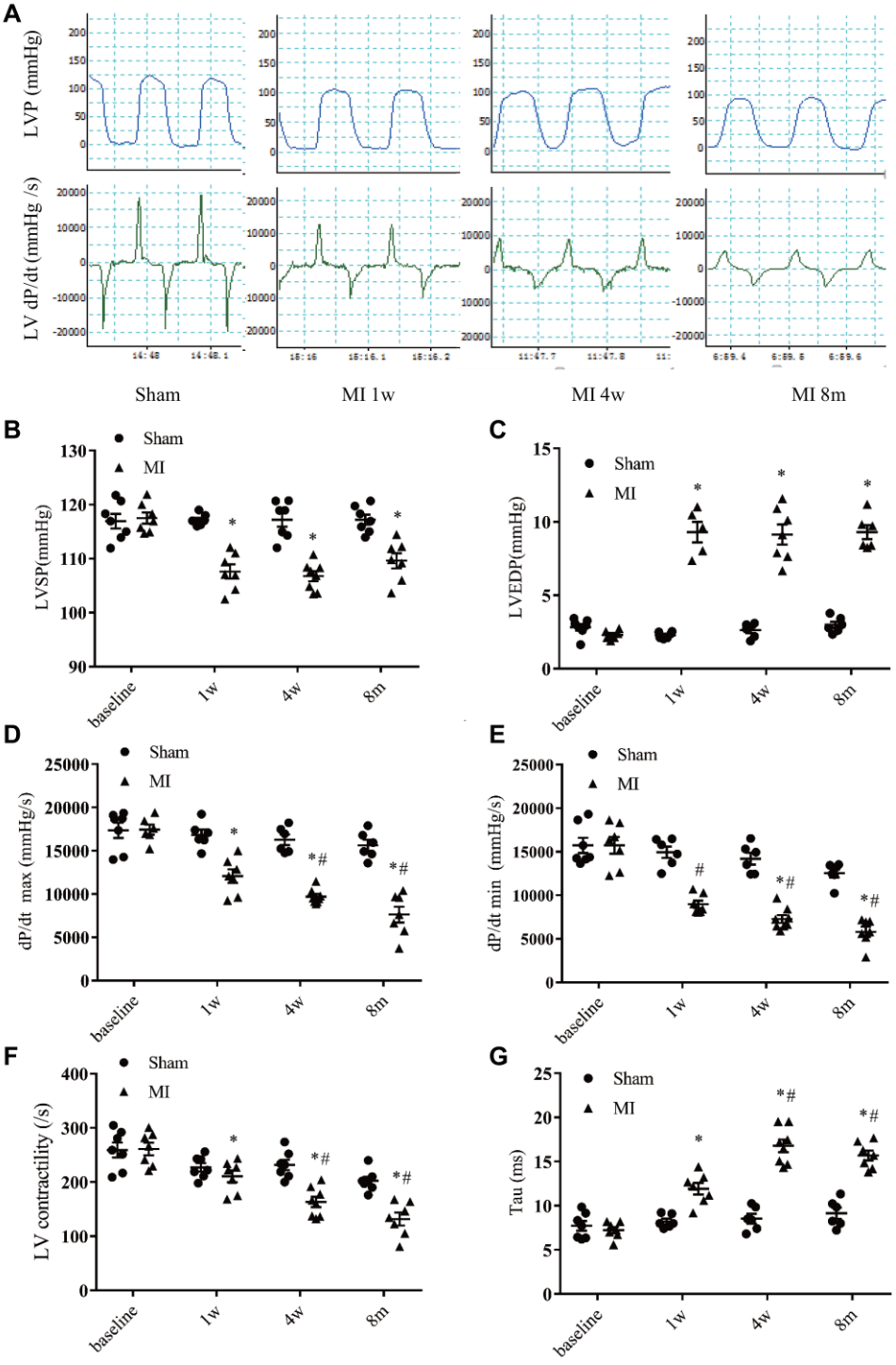

Figure 5. Hemodynamics assessment of left ventricular function. (**A**) Representative recordings of left ventricular (LV) pressure and pressure change rate (dp/dt). (**B**) LV systolic pressure. (**C**) LV end-diastolic pressure. (**D**) Maximum increasing rate of LV pressure (dp/dt max). (**E**) Maximum descending rate of the LV pressure (dp/dt min). (**F**) LV contractility index (dp/dt max divided by the pressure at the time of dp/dt max). (**G**) Exponential time constant of relaxation (Tau). $^{*}P < 0.05$ compared with the sham group. $^{\#}P < 0.05$ compared with the prior time point in the MI group. $n = 6–10$ at various time point.

approaches and observe their longer-term effects in animal models. However, the observational period of post-MI heart failure in the MI mouse model is generally 3–6 weeks and occasionally, a maximum of 1 year [14]. In the present study, we observed mice with MI for 8 months and analyzed their survival rate. Interestingly, the mortality rate of mice after MI decreased significantly 4 weeks after MI and most of

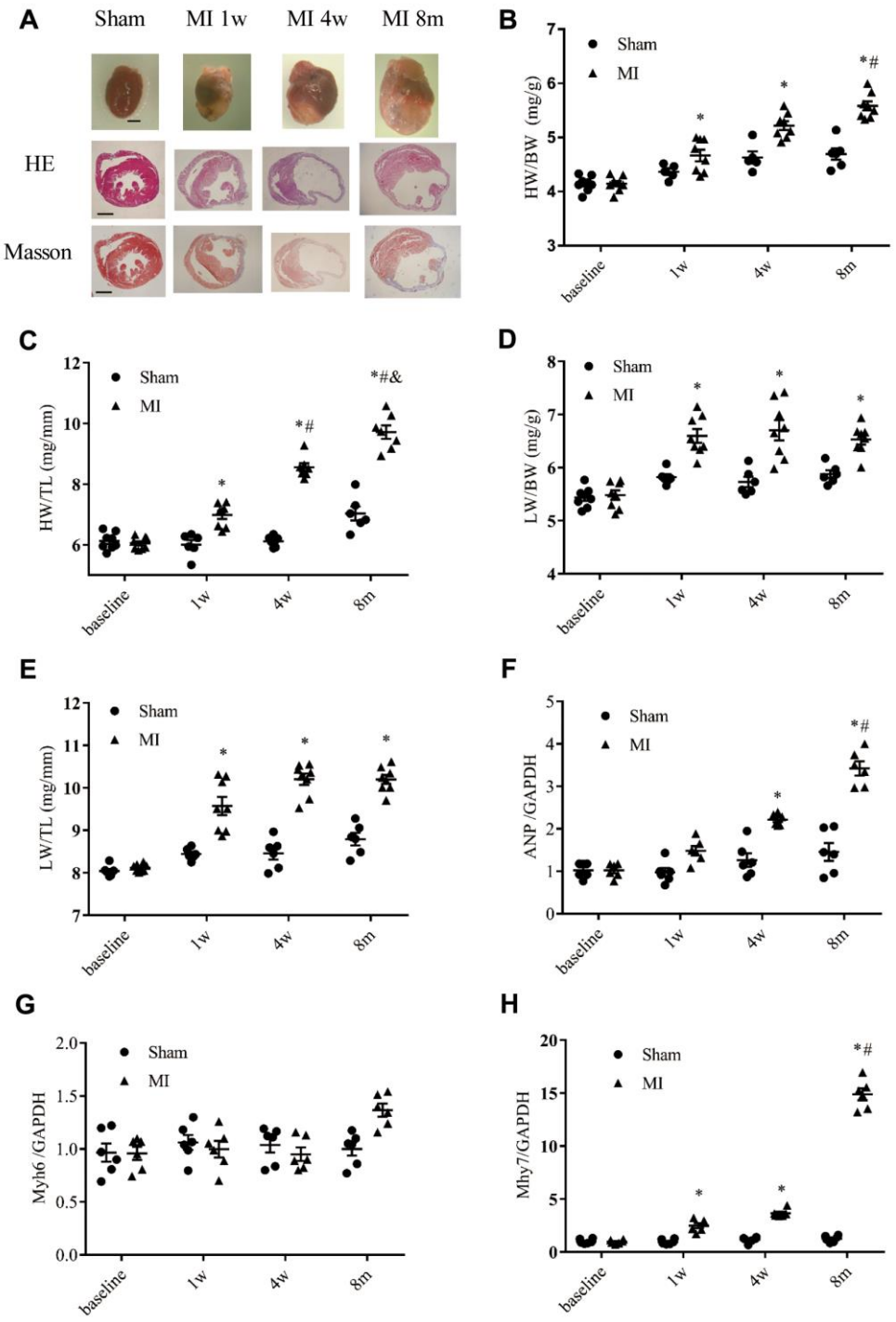

Figure 6. Cardiac remodeling validated by morphological and histological analysis. (**A**) Representative images of whole hearts and cross sections of hearts stained with hematoxylin-eosin staining (HE) and Masson's trichrome staining from different time points (scale bar = 2 mm). (**B**) Heart weight to body weight ratio (HW/BW). (**C**) Heart weight to tibia length ratio (HW/TL). (**D**) Lung weight to body weight ratio (LW/BW). (**E**) Lung weight to tibia length ratio (LW/TL); n = 8–10 at different time points. (**F**) Expression of the gene encoding ANP (atrial natrium peptide). (**G**) Expression of the gene encoding α-MHC (α-myosin heavy chain, Myh6). (**H**) Expression of β-MHC (Myh7); n = 6 at each time point. $^{*}P < 0.05$ vs. the corresponding time point in the sham group. $^{\#}P < 0.05$ compared with the prior time point in the MI group.

the surviving mice survived to 8 months with LV aneurysm. We also found that there are two dying windows, the first one occurred the first 10 days after MI, in which approximately one-quarter of mice died of cardiac rupture, which was in consistent with previous studies [15, 16]. The second one was 2–8 weeks after MI, in which an additional 20% of mice died of heart failure. Most of the mice that survived after 2 months survived until as long as 8 months, but they exhibited LV aneurysm, marked cardiac remodeling, decreased exercise tolerance and shortness of breath. During 1–8 months after MI, about 15% (4/27) mice died of decompensated heart failure (Figure 1F). Till to 8 months, about 40% (9/23) lived MI mice had obvious breath shortness and a decrease of running distance (fatigue), indicating that decompensated heart failure could occur in this 8-month MI model. These findings suggested that the long-term mouse MI model is ideal to test the interventional effects of novel therapies on cardiac remodeling.

Characterizing the transcriptional profiles in the hearts of mice at 8 months after MI might provide clues for identifying new therapeutic targets for heart failure. We observed a differential expression of the RNA Polymerase-1 pathway subunit in end-stage heart failure. RNA polymerase-1 is necessary in ribosomal RNA production, driving cell growth and driving cell division via its essential component of cellular protein synthesis machinery [17], and it also plays a vital role in determining the fate of cells when undergoing stress situations [18, 19]. It has been reported that dysregulation of polymerase-1 transcription is related to the etiology of human diseases [20].

The ability to repair injured tissue after MI is affected by numerous complex cellular and molecular pathways [21]. Our present GSEA analysis demonstrated that the up-regulated and down-regulated gene sets in the MI model were statistically enriched for growth and metabolism regulation, respectively. The activation of pathways promoting cell growth, proliferation, differentiation and regeneration, e.g., the WNT signaling pathway, were still increasing at 8 months after MI. Previous study has shown that active WNT signaling is markedly increased in the myocardium beginning 7 days post-MI, however, the observation time only lasted 3 weeks [22]. Unexpectedly, our findings showed that the WNT pathway activation was still increasing at 8 months after MI. Activation of WNT pathway may be one of the important factors by which long-term MI leads to exacerbated cardiac dysfunction. We found that CTNNB1 is the only top ranked differentially expressed gene located at the core of the network. Previous studies have shown that CTNNB1 is mostly related to the occurrence and development of tumors, including Craniopharyngioma [23], Hepatocellular [24] and Gastric cancer [25], Studies have also shown that CTNNB1 has an important relationship with heart development [26]. WNT/CTNNB1 are required for cardiogenesis, but the specific role of CTNNB1 in cardiac repair after MI remains unclear. Thus, CTNNB1 should be used as a potential target gene for the further mechanistic approaches. Another pathway that was significantly upregulated in the MI group was the Integrin signaling pathway, which has been proved to participate in multiple critical cellular processes in cardiomyocytes including adhesion, extracellular matrix organization, signaling, survival, and proliferation. Integrins are mechano-transducers and are particularly relevant for a contracting muscle cell, and they translate mechanical information to biochemical information [27]. We found that the most highly up-regulated gene in the integrin pathway was COL8A1, which has been confirmed to be involved in the progression of cardiac dilation [28] and TAC-induced cardiac pathological remodeling [29]. Due to the small size of the mouse heart, we used the whole heart rather than a special portion of the heart to perform transcript analysis. Therefore, it is unclear where the altered gene expression occurred. As shown in Supplementary Figure 5, the deposition of β-catenin and collagen-8 protein occurred in both the infarct area and border area sections in mice at 8 months post-MI, suggesting that the altered expression of their corresponding coding genes, CTNNB1 and COL8A1 occur in both the infarct and border area. Our findings indicated that CTNNB1 and COL8A1 may play an important role in the cardiac remodeling progress of long term MI. Similarly, we found that the activity of either fatty acid or oxidative phosphorylation pathways mostly processed by mitochondrial was still in decreasing phase even at 8 months after MI, and this long term persistent dysregulation of energy metabolism may provide targets for improving heart failure. Oxidative metabolism in mitochondria is the main energy source of the heart, and maladjustment to myocardial energy stress leads to metabolism dysfunction and in turn exacerbates a vicious cycle that increases myocardial damage [30]. Overall, efforts to sustain energy homeostasis are promising therapeutic strategies to combat heart failure.

Differential gene analysis using PCA showed that 95 genes were continuously differentially regulated during the 8-month monitoring period. GGO and EGO analyses indicated that genes associated with cytokine pathways and metabolic processes were commonly regulated at 1 month and 8 months after MI. Cytokine signaling is an important part of regulator processes throughout the human body as cytokines bind to receptors on target cells and activate a cascade of intercellular signals, such as the protein kinase

transduction cascade [31], and these signals may have a sustained effect on post-MI cardiac remodeling.

In summary, our findings indicated that most mice with chronic MI and marked cardiac remodeling and LV aneurysm can survive for more than 8 months. The time-course of cardiac remodeling was noninvasively evaluated with ECG and echocardiography, while molecular and histological changes were examined at the indicated time points. We first addressed the transcriptomic characteristics at 8 months after MI by transcriptomic profiling analysis using RNA-seq. We also compared the similarities and differences of early and advanced transcriptomic expression by analyzing published sequencing data. Our identification of differentially expressed genes and pathways at various time points after MI will ultimately facilitate the development of new therapeutics for chronic heart failure.

MATERIALS AND METHODS

MI Model

The experiments were performed in accordance with our institution's guidelines for animal research that conform to the Guide for the Care and Use of Laboratory Animals (National Institutes of Health Publication, 8th Edition, 2011). Approval for this study was granted by our university's ethics review board. Male C57BL/6 mice aged 10–12 weeks and weighing 25–35 g were intraperitoneal anesthetized with a mixture of xylazine (5 mg/kg) and ketamine (100 mg/kg), intubated with PE-90 tubing, and ventilated with room air using a mouse mini-ventilator. The respiration rate was set between 110–130 times/minute. Thoracotomy was performed between the 3rd and 4th rib to expose the left coronary artery (LCA). An 8–0 nylon suture was then placed around the LCA at 2 mm from the tip of the left auricle and the vessel was ligated as previously described [32, 33]. Coronary occlusion was confirmed by ST segment elevation on the ECG monitor [34], and only mice with a ST elevation in lead II >1/2 of R wave were included in this study.

At the indicated time points, the mice were sacrificed by an overdose of anesthetic (pentobarbital sodium;150 mg·kg−1, i.p.), and their hearts and lungs were harvested for further analysis. Myocardial infarct size was determined using TTC staining [35].

Exercise exhaustion test

After 3 days of acclimatization to treadmill exercise, mice from the sham 8 m and MI 8 m groups were forced to receive an exhaustion test. Animals ran uphill (20°) on the treadmill (ShangHai Biowill Co., Ltd.) starting at a warm-up speed of 5 m/min for 4 min, after which speed was increased to 14 m/min for 2 min. Every subsequent 2 min, the speed was increased by 2 m/min until the animal was exhausted. Exhaustion was defined as the inability of the animal to return to running within 10 sec of direct contact with an electric-stimulus grid. Total running distance in a period from starting to the occurrence of exhaustion for each mouse was calculated.

Echocardiography

Transthoracic echocardiography measurements were performed using the VisualSonics Vevo 2100 high-resolution ultrasound imaging system (Fujifilm VisualSonics, Inc., Toronto, Canada) with a MS400 transducer. Ultrasound was performed to evaluate cardiac function at the indicated time points (baseline, 1-week, 4-week and 8-months in the post-MI or sham groups). The mice were immobilized with isoflurane anesthesia and placed in a supine position on a heated pad. Heart rates were approximately 400–500 beats/minutes under anaesthesia, A two-dimensional short-axis view of the LV for guided M-mode was obtained perpendicular to the ventricular septum and posterior wall at the tip of the mitral leaflets. The LVESd, LVEDd and LV wall thickness were directly measured, while the LVEF and LVFS were automatically obtained using the calculation system.

Invasive LV hemodynamics

LV hemodynamics were evaluated before the animals were sacrificed using Power Lab software (blood pressure module; AD Instruments, Australia) [36, 37]. Briefly, mice from each group were anesthetized with pentobarbital (light anesthesia with 30 mg/kg, ip), and were ventilated. A Millar catheter (Millar Instruments, Inc., Houston, TX) was inserted via the right carotid artery and carefully introduced into the LV to measure the LVSP, LVEDP, and maximum rates of change in the LV pressure (dp/dt max and dp/dt min, respectively). Both the contractility index and the exponential time constant of relaxation (τ) were calculated using the Blood Pressure Module software.

Histological analyses

We performed all histological analyses on fixed (4% paraformaldehyde) heart tissue. After fixation, the samples underwent a series of dehydrations, and 4-μm sections were obtained after the samples were embedded in paraffin blocks. HE (hematoxylin-eosin) staining was used to determine cardiomyocyte morphology [38]. Myocardial fibrosis and old myocardial infarct size were assessed with Masson's trichrome staining [39].

Immunohistochemical staining was performed in different sections of the infarcted hearts to determine where the altered gene expression occurred according to a previously described protocol [40].

Immunohistochemistry

Heart tissues were harvested from sham 8m and MI 8m mice, fixed in 4% paraformaldehyde and embedded in paraffin. Then 4 μm sections were obtained for immunostaining. After antigen retrieval by heating in citrate buffer (pH 6.0), the sections were incubated with primary antibodies overnight at 4°C. β-catenin (1:100, Santa Cruz, CA, USA), collagen-8 (1:100, Abcam, MA, USA). The sections were incubated with an HRPlabeled secondary antibody for 1 hour. Then Dako EVision + System-HRP (DAB) were used to visualize the indicated protein staining. Images were captured using an upright microscope (Olympus, Japan).

Real-time PCR

Total tissue RNA was extracted from hearts with a total RNA isolation system (R4369-01, Omega, USA). The sequences of the primers were designed by Primer Premiers 6.0. We measured the relative expression levels of genes encoding alpha-myosin heavy chain gene (α-MHC, Myh6), beta-myosin heavy chain gene (β-MHC, Myh7), atrial natriuretic peptide gene (ANP) and glyceraldehyde-3-phosphate dehydrogenase (GAPDH) in hearts harvested from mice with MI or sham-operated mice using the TaqMan real-time PCR method and a Quantitect SYBR Green RT-PCR kit (DRR420A, Takara, Japan), as described elsewhere [41].

Bioinformatics analysis

For each sample, the raw reads obtained from the sequencing instrument were processed to obtain clean reads by removing sequencing adapters and low quality. High-quality sequences were aligned to the *Mus musculus* 10 database using Hisat2 2.0.5 software. Subsequently, StringTie 1.3.3b software was employed to assemble and quantify the transcripts, from which we got a raw gene count matrix. Differential expression analysis was conducted using software DESeq2 1.20.0 software. PCA performed by R was used for difference pre-analysis and sample classification. The WGCNA R software package was used to perform analysis on various aspects of the weighted correlation network [42]. We screened 75% of the gene based on the absolute deviation of the median (MAD), and genes with an MAD at least greater than 1 (4437 genes) were subjected to cluster analysis. GSEA was performed to analyze ranked lists of all available genes with no threshold, and our data were analyzed by gene sets from specialized mouse databases (GSKB; http://ge-lab.org/gskb/). The Protein-protein interactions network (PPI) was analyzed by using String database (Version 11.0). The Visualized network was mapped using Cytoscape software and CytoHubba was used to calculate the top-ranked nodes in the network [43].

Statistical analysis

All the data are expressed as the mean ± standard error of mean (SEM), and significant differences between two experimental groups were calculated using the *t* test. Survival rates were calculated according to the Kaplan–Meier method and *P* values less than 0.05 were considered to be statistically significant [44].

Statement

No human studies were carried out by the authors for this article.

Availability of data and materials

The datasets used and/or analyzed during the current study are available from the corresponding author on reasonable request.

Abbreviations

CHF: chronic heart failure; MI: myocardial infarction; LV: left ventricular; RNA-seq: RNA sequencing; PCA: Principal Component Analysis; GO: Gene Ontology; WGCNA: Weighted Gene Co-expression Network Analysis; GSEA: Gene Set Enrichment Analysis; ECG: electrocardiogram; LCA: left coronary artery; TTC: Triphenyl tetrazolium chloride; LVESd: Left ventricular end-systolic diameters; LVEDd: Left ventricular end-diastolic diameters; LVFS: Left ventricular fractional shortening; LVEF: Left ventricular ejection fraction; LVSP: Left ventricular systolic pressure; LVEDP: Left ventricular end diastolic pressure; dp/dt max/min: maximum/minimum rates of change in the LV pressure; τ: the exponential time constant of relaxation; HE: hematoxylin-eosin; Myh6: alpha-myosin heavy chain gene; Myh7: beta-myosin heavy chain gene; ANP: atrial natriuretic peptide gene; GAPDH: glyceraldehyde-3-phosphate dehydrogenase; MAD: absolute deviation of the median; SEM: standard error of mean; LDHA/B: lactate dehydrogenase A/B; MDH2: malate dehydrogenase 2; PDK4/2: pyruvate dehydrogenase kinase 4/2; PDP1: pyruvate dehydrogenase phosphatase catalytic subunit 1; PDHA1/2: pyruvate dehydrogenase E1 alpha 1/2 subunits; EGO: Enrich Gene Ontology; GGO: Group Gene Ontology

AUTHOR CONTRIBUTIONS

(I) Conception and experiment design: Yulin Liao, Qiancheng Wang. (II) Experiments performing and data collection: Yingqi Zhu, Qiancheng Wang, Hairuo Lin, Kaitong Chen. (III) Data analysis and interpretation: Yingqi Zhu, Qiancheng Wang, Hairuo Lin, Cankun Zheng, Lin Chen, Siyuan Ma, Yulin Liao, Jianping Bin, Wangjun Liao. (IV) Manuscript writing and revising: Yingqi Zhu, Qiancheng Wang, Yulin Liao

CONFLICTS OF INTEREST

All authors declared no conflict of interest.

FUNDING

This work was supported by grants from the National Natural Science Foundation of China (81570464 to Y.L.), the Joint Funds of the National Natural Science Foundation of China (U1908205 to Y.L.),the Municipal Planning Projects of Scientific Technology of Guangzhou (201804020083 to Y.L.), the Key program of Natural Science Foundation of Guangdong Province (2018B0303110008 to Y.L.), the Key Research & Development Program of Guangzhou Regenerative Medicine and Health Guangdong Laboratory (2018GZR110104001to Y.L.), and Open Project Fund of the State Key Laboratory of Organ Failure Prevention and Treatment(201902 to J.X, 202001to Z.C).

REFERENCES

1. Benjamin EJ, Muntner P, Alonso A, Bittencourt MS, Callaway CW, Carson AP, Chamberlain AM, Chang AR, Cheng S, Das SR, Delling FN, Djousse L, Elkind MSV, et al, and American Heart Association Council on Epidemiology and Prevention Statistics Committee and Stroke Statistics Subcommittee. Heart Disease and Stroke Statistics-2019 Update: A Report From the American Heart Association. Circulation. 2019; 139:e56–e528. https://doi.org/10.1161/CIR.0000000000000659 PMID:30700139

2. Mudd JO, Kass DA. Reversing chronic remodeling in heart failure. Expert Rev Cardiovasc Ther. 2007; 5:585–98. https://doi.org/10.1586/14779072.5.3.585 PMID:17489680

3. Braunwald E. The war against heart failure: the Lancet lecture. Lancet. 2015; 385:812–24. https://doi.org/10.1016/S0140-6736(14)61889-4 PMID:25467564

4. Cahill TJ, Choudhury RP, Riley PR. Heart regeneration and repair after myocardial infarction: translational opportunities for novel therapeutics. Nat Rev Drug Discov. 2017; 16:699–717. https://doi.org/10.1038/nrd.2017.106 PMID:28729726

5. Vallejo-Vaz AJ, Robertson M, Catapano AL, Watts GF, Kastelein JJ, Packard CJ, Ford I, Ray KK. Low-Density Lipoprotein Cholesterol Lowering for the Primary Prevention of Cardiovascular Disease Among Men With Primary Elevations of Low-Density Lipoprotein Cholesterol Levels of 190 mg/dL or Above: Analyses From the WOSCOPS (West of Scotland Coronary Prevention Study) 5-Year Randomized Trial and 20-Year Observational Follow-Up. Circulation. 2017; 136:1878–91. https://doi.org/10.1161/CIRCULATIONAHA.117.027966 PMID:28877913

6. Flurkey K, Currer J, Harrison D. The Mouse in Aging Research. The Mouse in Biomedical Research. 2007; 3.

7. Chen Z, Xie J, Hao H, Lin H, Wang L, Zhang Y, Chen L, Cao S, Huang X, Liao W, Bin J, Liao Y. Ablation of periostin inhibits post-infarction myocardial regeneration in neonatal mice mediated by the phosphatidylinositol 3 kinase/glycogen synthase kinase 3beta/cyclin D1 signalling pathway. Cardiovasc Res. 2017; 113:620–32. https://doi.org/10.1093/cvr/cvx001 PMID:28453729

8. Xuan W, Wu B, Chen C, Chen B, Zhang W, Xu D, Bin J, Liao Y. Resveratrol improves myocardial ischemia and ischemic heart failure in mice by antagonizing the detrimental effects of fractalkine*. Crit Care Med. 2012; 40:3026–33. https://doi.org/10.1097/CCM.0b013e31825fd7da PMID:22926332

9. Boon RA, Dimmeler S. MicroRNAs in myocardial infarction. Nat Rev Cardiol. 2015; 12:135–42. https://doi.org/10.1038/nrcardio.2014.207 PMID:25511085

10. Nomura S, Satoh M, Fujita T, Higo T, Sumida T, Ko T, Yamaguchi T, Tobita T, Naito AT, Ito M, Fujita K, Harada M, Toko H, et al. Cardiomyocyte gene programs encoding morphological and functional signatures in cardiac hypertrophy and failure. Nat Commun. 2018; 9:4435. https://doi.org/10.1038/s41467-018-06639-7 PMID:30375404

11. Duan Q, McMahon S, Anand P, Shah H, Thomas S, Salunga HT, Huang Y, Zhang R, Sahadevan A, Lemieux ME, Brown JD, Srivastava D, Bradner JE, et al. BET bromodomain inhibition suppresses innate inflammatory and profibrotic transcriptional networks in heart failure. Sci Transl Med. 2017; 9:eaah5084. https://doi.org/10.1126/scitranslmed.aah5084

PMID:28515341

12. Dargie HJ. Effect of carvedilol on outcome after myocardial infarction in patients with left-ventricular dysfunction: the CAPRICORN randomised trial. Lancet. 2001; 357:1385–90. https://doi.org/10.1016/s0140-6736(00)04560-8 PMID:11356434

13. Flather MD, Yusuf S, Køber L, Pfeffer M, Hall A, Murray G, Torp-Pedersen C, Ball S, Pogue J, Moyé L, Braunwald E. Long-term ACE-inhibitor therapy in patients with heart failure or left-ventricular dysfunction: a systematic overview of data from individual patients. ACE-Inhibitor Myocardial Infarction Collaborative Group. Lancet. 2000; 355:1575–81. https://doi.org/10.1016/s0140-6736(00)02212-1 PMID:10821360

14. Pons S, Fornes P, Hagege AA, Heudes D, Giudicelli JF, Richer C. Survival, haemodynamics and cardiac remodelling follow up in mice after myocardial infarction. Clin Exp Pharmacol Physiol. 2003; 30:25–31. https://doi.org/10.1046/j.1440-1681.2003.03784.x PMID:12542449

15. Gao XM, Xu Q, Kiriazis H, Dart AM, Du XJ. Mouse model of post-infarct ventricular rupture: time course, strain- and gender-dependency, tensile strength, and histopathology. Cardiovasc Res. 2005; 65:469–77. https://doi.org/10.1016/j.cardiores.2004.10.014 PMID:15639486

16. Muthuramu I, Jacobs F, Singh N, Gordts SC, De Geest B. Selective homocysteine lowering gene transfer improves infarct healing, attenuates remodelling, and enhances diastolic function after myocardial infarction in mice. PLoS One. 2013; 8:e63710. https://doi.org/10.1371/journal.pone.0063710 PMID:23675503

17. Goodfellow SJ, Zomerdijk JC. Basic mechanisms in RNA polymerase I transcription of the ribosomal RNA genes. Subcell Biochem. 2013; 61:211–36. https://doi.org/10.1007/978-94-007-4525-4_10 PMID:23150253

18. Fernandez-Tornero C. RNA polymerase I activation and hibernation: unique mechanisms for unique genes. Transcription. 2018; 9:248–54. https://doi.org/10.1080/21541264.2017.1416267 PMID:29372670

19. Russell J, Zomerdijk JC. RNA-polymerase-I-directed rDNA transcription, life and works. Trends Biochem Sci. 2005; 30:87–96. https://doi.org/10.1016/j.tibs.2004.12.008 PMID:15691654

20. Hannan KM, Sanij E, Rothblum LI, Hannan RD, Pearson RB. Dysregulation of RNA polymerase I transcription during disease. Biochim Biophys Acta. 2013; 1829:342–60. https://doi.org/10.1016/j.bbagrm.2012.10.014 PMID:23153826

21. Curley D, Lavin Plaza B, Shah AM, Botnar RM. Molecular imaging of cardiac remodelling after myocardial infarction. Basic Res Cardiol. 2018; 113:10. https://doi.org/10.1007/s00395-018-0668-z PMID:29344827

22. Oerlemans MI, Goumans MJ, van Middelaar B, Clevers H, Doevendans PA, Sluijter JPG. Active Wnt signaling in response to cardiac injury. Basic Res Cardiol. 2010; 105:631–41. https://doi.org/10.1007/s00395-010-0100-9 PMID:20373104

23. Müller HL, Merchant TE, Warmuth-Metz M, Martinez-Barbera JP, Puget S. Craniopharyngioma. Nat Rev Dis Primers. 2019; 5:75. https://doi.org/10.1038/s41572-019-0125-9 PMID:31699993

24. Zucman-Rossi J, Villanueva A, Nault JC, Llovet JM. Genetic Landscape and Biomarkers of Hepatocellular Carcinoma. Gastroenterology. 2015; 149:1226–39.e4. https://doi.org/10.1053/j.gastro.2015.05.061 PMID:26099527

25. Melucci E, Casini B, Ronchetti L, Pizzuti L, Sperati F, Pallocca M, De Nicola F, Goeman F, Gallo E, Amoreo CA, Sergi D, Terrenato I, Vici P, et al. Expression of the Hippo transducer TAZ in association with WNT pathway mutations impacts survival outcomes in advanced gastric cancer patients treated with first-line chemotherapy. J Transl Med. 2018; 16:22. https://doi.org/10.1186/s12967-018-1385-y PMID:29402328

26. Norden J, Kispert A. Wnt/Ctnnb1 signaling and the mesenchymal precursor pools of the heart. Trends Cardiovasc Med. 2012; 22:118–22. https://doi.org/10.1016/j.tcm.2012.07.006 PMID:22902180

27. Israeli-Rosenberg S, Manso AM, Okada H, Ross RS. Integrins and integrin-associated proteins in the cardiac myocyte. Circ Res. 2014; 114:572–86. https://doi.org/10.1161/CIRCRESAHA.114.301275 PMID:24481847

28. Gil-Cayuela C, Roselló-LLetí E, Ortega A, Tarazón E, Triviño JC, Martínez-Dolz L, González-Juanatey JR, Lago F, Portolés M, Rivera M. New Altered Non-Fibrillar Collagens in Human Dilated Cardiomyopathy: Role in the Remodeling Process. PLoS One. 2016;

11:e0168130.
https://doi.org/10.1371/journal.pone.0168130
PMID:27936202

29. Wang HB, Huang R, Yang K, Xu M, Fan D, Liu MX, Huang SH, Liu LB, Wu HM, Tang QZ. Identification of differentially expressed genes and preliminary validations in cardiac pathological remodeling induced by transverse aortic constriction. Int J Mol Med. 2019; 44:1447–61.
https://doi.org/10.3892/ijmm.2019.4291
PMID:31364721

30. Zhou B, Tian R. Mitochondrial dysfunction in pathophysiology of heart failure. J Clin Invest. 2018; 128:3716–26.
https://doi.org/10.1172/JCI120849
PMID:30124471

31. Bartekova M, Radosinska J, Jelemensky M, Dhalla NS. Role of cytokines and inflammation in heart function during health and disease. Heart Fail Rev. 2018; 23:733–58.
https://doi.org/10.1007/s10741-018-9716-x
PMID:29862462

32. Wang Y, Chen Y, Yan Y, Li X, Chen G, He N, Shen S, Chen G, Zhang C, Liao W, Liao Y, Bin J. Loss of CEACAM1, a Tumor-Associated Factor, Attenuates Post-infarction Cardiac Remodeling by Inhibiting Apoptosis. Sci Rep. 2016; 6:21972.
https://doi.org/10.1038/srep21972
PMID:26911181

33. Xuan W, Liao Y, Chen B, Huang Q, Xu D, Liu Y, Bin J, Kitakaze M. Detrimental effect of fractalkine on myocardial ischaemia and heart failure. Cardiovasc Res. 2011; 92:385–93.
https://doi.org/10.1093/cvr/cvr221
PMID:21840883

34. Feng G, Yan Z, Li C, Hou Y. microRNA-208a in an early stage myocardial infarction rat model and the effect on cAMP-PKA signaling pathway. Mol Med Rep. 2016; 14:1631–35.
https://doi.org/10.3892/mmr.2016.5402
PMID:27314868

35. Dai Y, Song J, Li W, Yang T, Yue X, Lin X, Yang X, Luo W, Guo J, Wang X, Lai S, Andrade KC, Chang J. RhoE Fine-Tunes Inflammatory Response in Myocardial Infarction. Circulation. 2019; 139:1185–98.
https://doi.org/10.1161/CIRCULATIONAHA.118.033700
PMID:30586715

36. Wei X, Wu B, Zhao J, Zeng Z, Xuan W, Cao S, Huang X, Asakura M, Xu D, Bin J, Kitakaze M, Liao Y. Myocardial Hypertrophic Preconditioning Attenuates Cardiomyocyte Hypertrophy and Slows Progression to Heart Failure Through Upregulation of S100A8/A9. Circulation. 2015; 131:1506–17.
https://doi.org/10.1161/CIRCULATIONAHA.114.013789
PMID:25820336

37. Xie J, Cui K, Hao H, Zhang Y, Lin H, Chen Z, Huang X, Cao S, Liao W, Bin J, Kitakaze M, Liao Y. Acute hyperglycemia suppresses left ventricular diastolic function and inhibits autophagic flux in mice under prohypertrophic stimulation. Cardiovasc Diabetol. 2016; 15:136.
https://doi.org/10.1186/s12933-016-0452-z
PMID:27659110

38. Hua Y, Chen H, Zhao X, Liu M, Jin W, Yan W, Wu Y, Tan Z, Fan H, Wu Y, Xie L, Zhang W, Liu B, Zhou Y. Alda–1, an aldehyde dehydrogenase–2 agonist, improves long–term survival in rats with chronic heart failure following myocardial infarction. Mol Med Rep. 2018; 18:3159–66.
https://doi.org/10.3892/mmr.2018.9309
PMID:30066916

39. Hua J, Liu Z, Liu Z, An D, Lai W, Zhan Q, Zeng Q, Ren H, Xu D. Metformin Increases Cardiac Rupture After Myocardial Infarction via the AMPK-MTOR/PGC-1α Signaling Pathway in Rats with Acute Myocardial Infarction. Med Sci Monit. 2018; 24:6989–7000.
https://doi.org/10.12659/MSM.910930
PMID:30275441

40. Hao H, Li X, Li Q, Lin H, Chen Z, Xie J, Xuan W, Liao W, Bin J, Huang X, Kitakaze M, Liao Y. FGF23 promotes myocardial fibrosis in mice through activation of β-catenin. Oncotarget. 2016; 7:64649–64.
https://doi.org/10.18632/oncotarget.11623
PMID:27579618

41. Lin H, Li Y, Zhu H, Wang Q, Chen Z, Chen L, Zhu Y, Zheng C, Wang Y, Liao W, Bin J, Kitakaze M, Liao Y. Lansoprazole alleviates pressure overload-induced cardiac hypertrophy and heart failure in mice by blocking the activation of beta-catenin. Cardiovasc Res. 2020; 116:101–13.
https://doi.org/10.1093/cvr/cvz016
PMID:30689763

42. Langfelder P, Horvath S. WGCNA: an R package for weighted correlation network analysis. BMC Bioinformatics. 2008; 9:559.
https://doi.org/10.1186/1471-2105-9-559
PMID:19114008

43. Chin CH, Chen SH, Wu HH, Ho CW, Ko MT, Lin CY. cytoHubba: identifying hub objects and sub-networks from complex interactome. BMC Syst Biol. 2014 (Suppl 4); 8:S11.
https://doi.org/10.1186/1752-0509-8-S4-S11
PMID:25521941

44. Chen Y, Zhang C, Shen S, Guo S, Zhong L, Li X, Chen G, Chen G, He X, Huang C, He N, Liao W, Liao Y, Bin J. Ultrasound-targeted microbubble destruction

enhances delayed BMC delivery and attenuates post-infarction cardiac remodelling by inducing engraftment signals. Clin Sci (Lond). 2016; 130:2105–20.
https://doi.org/10.1042/CS20160085
PMID:27609823

SUPPLEMENTARY MATERIALS

Supplementary Figures

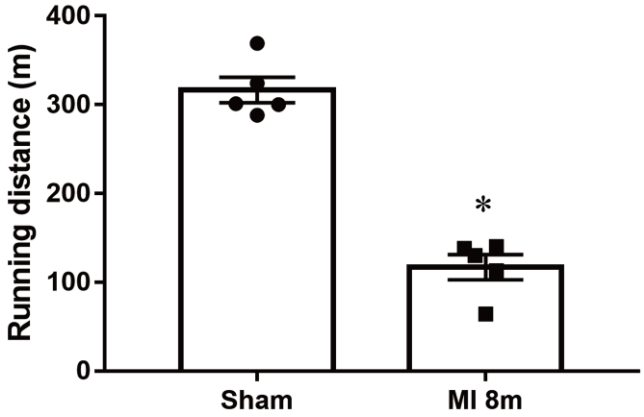

Supplementary Figure 1. Running distance during exercise exhaustion test in mice at 8 months after MI.

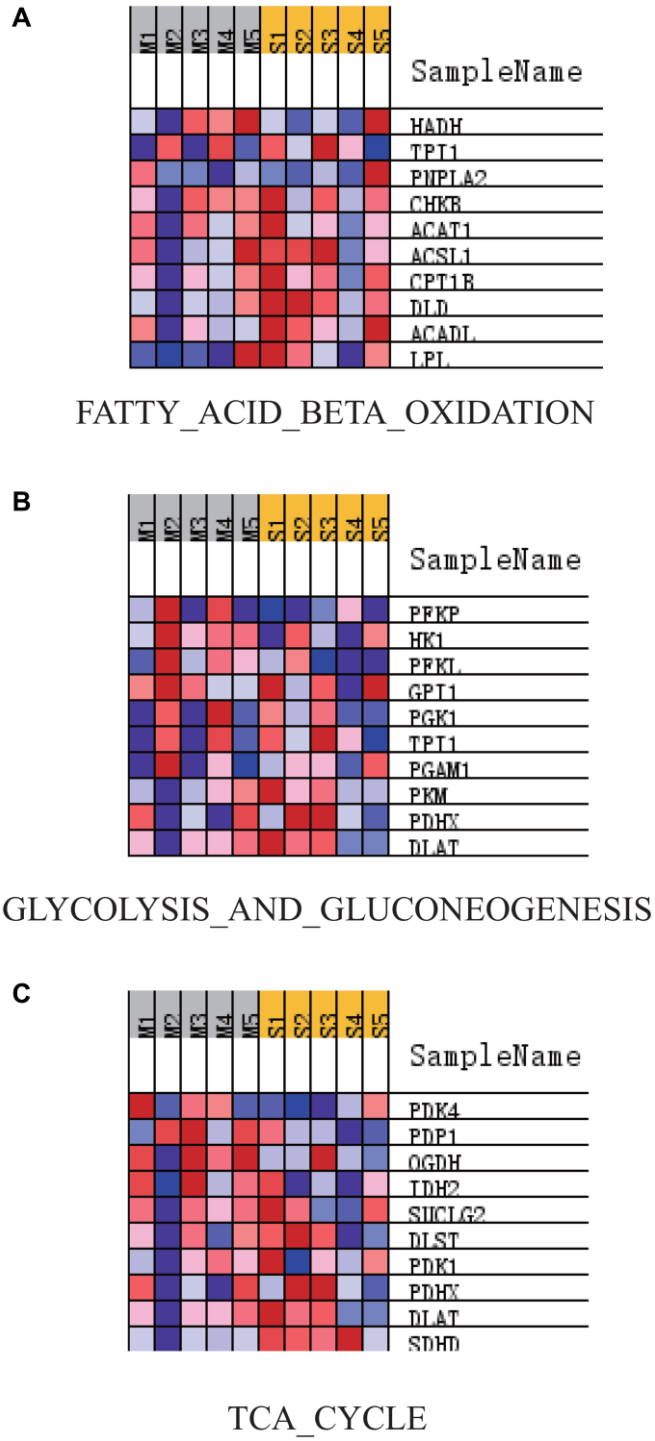

Supplementary Figure 2. Downregulated pathways identified by GSEA analysis. (**A**) Heatmap of the enriched genes in the fatty acid beta oxidation pathway. (**B**) Heatmap of the enriched genes in the glycolysis and gluconeogenesis pathway. (**C**) Heatmap of the enriched genes in the TCA cycle pathway.

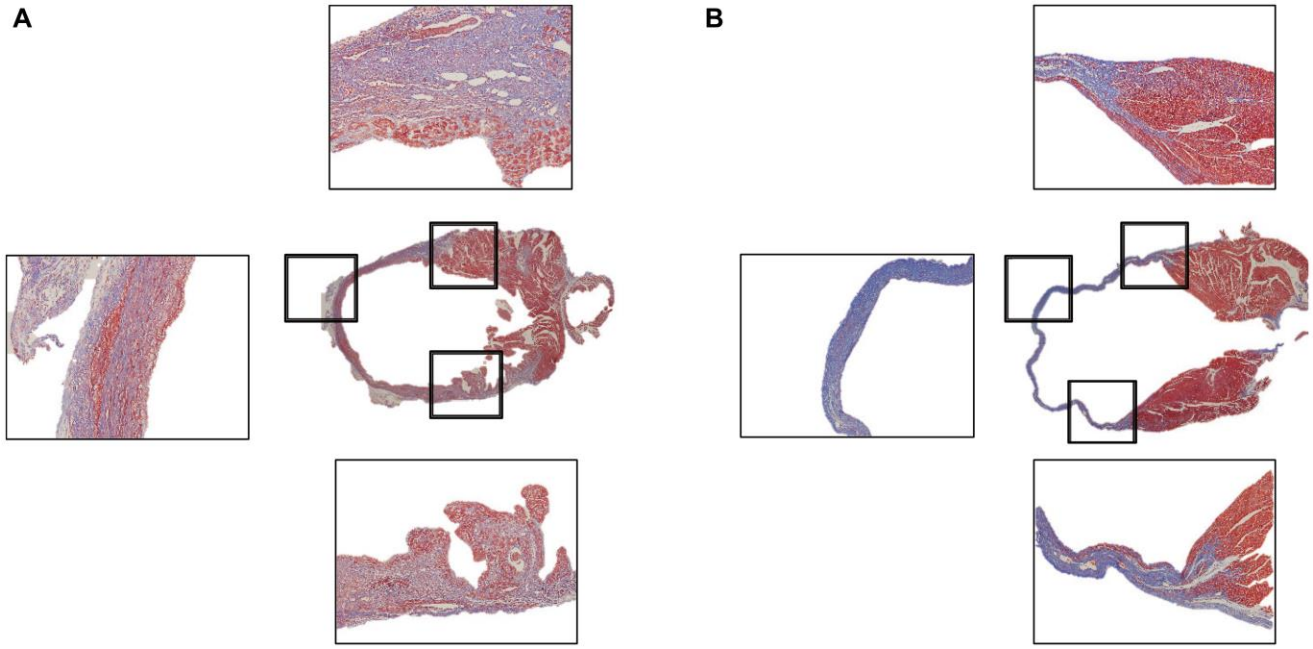

Supplementary Figure 3. Cardiac remodeling validated by detailed morphological and histological analysis. (**A**) Representative longitudinal section pictures of heart stained with Masson's trichrome staining from 4 weeks after myocardial infarction (MI). (**B**) Representative longitudinal section pictures of heart stained with Masson's trichrome staining from 8 months after MI. Zoomed frames indicated the areas around the infarct sites after MI.

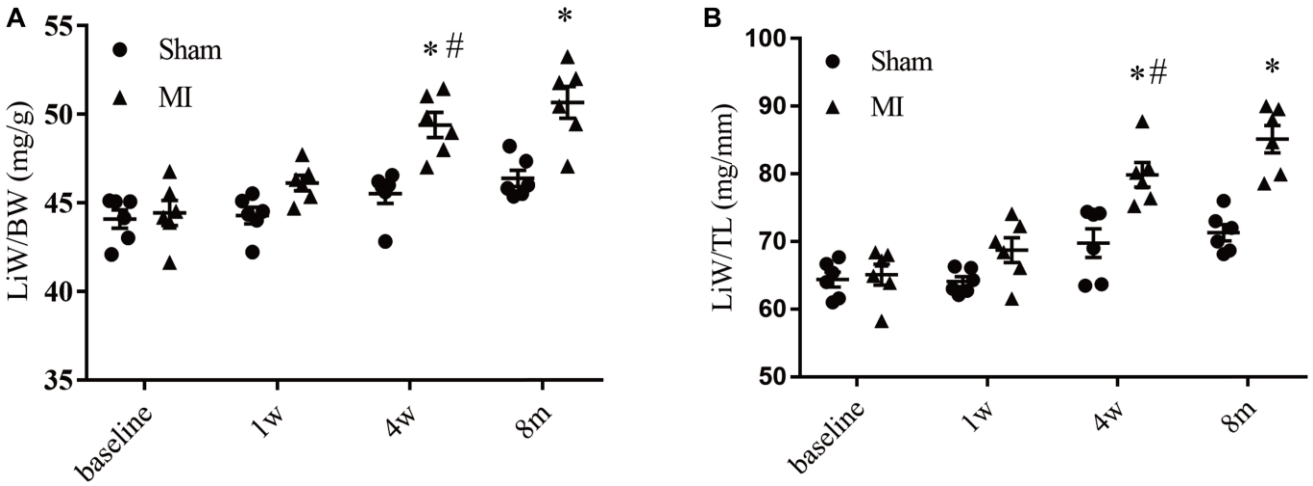

Supplementary Figure 4. The liver weight in mice at 8 months after MI. (**A**) The liver weight (mg) to body weight (g) ratio (LiW/BW). (**B**) The liver weight (mg) to tibia length (mm) ratio (LiW/TL). $^{*}P < 0.05$ vs. the corresponding time point in the sham group. $^{\#}P < 0.05$ compared with the prior time point in the MI group.

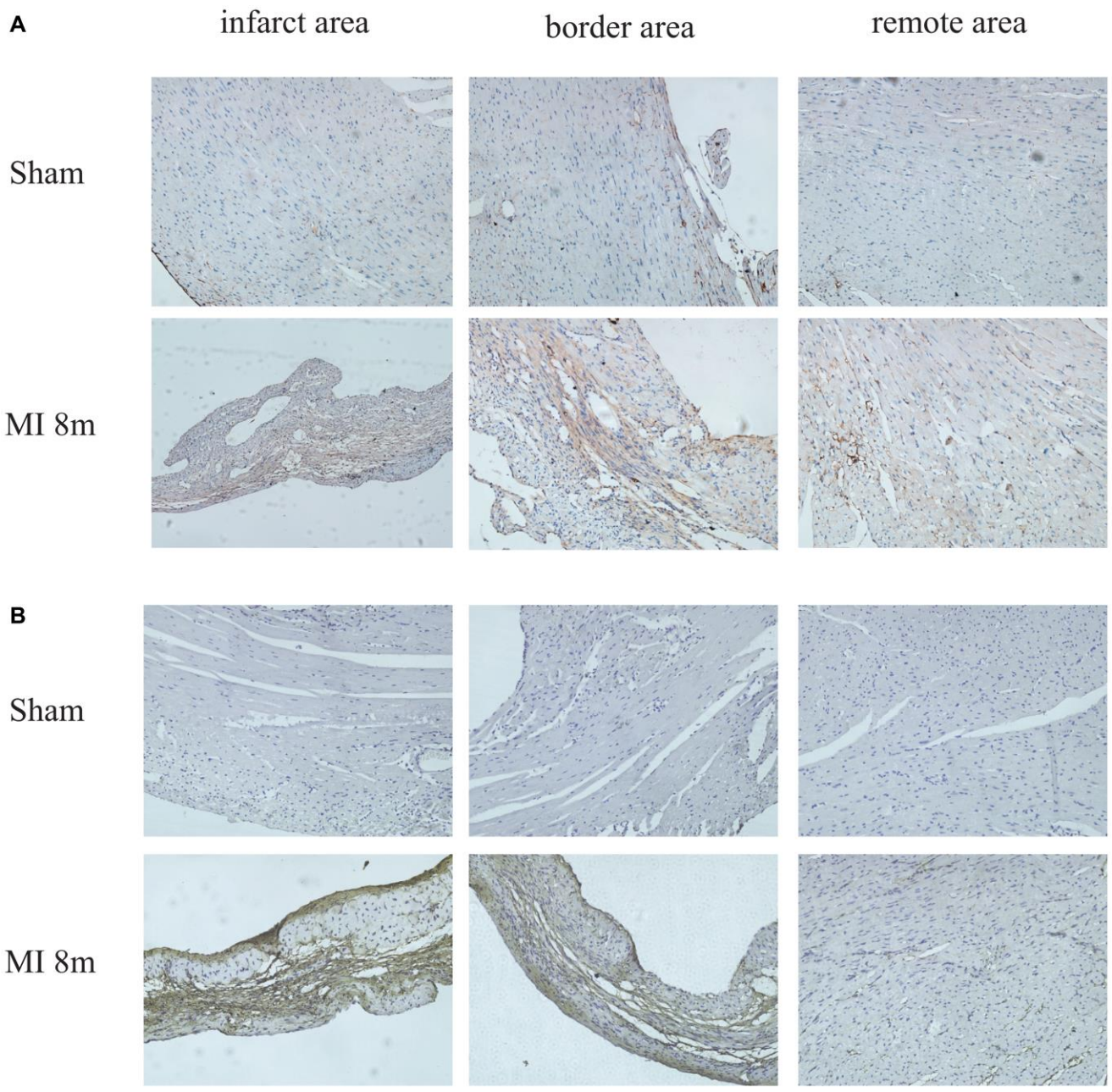

Supplementary Figure 5. Representative immunohistochemical staining graphs in the hearts. (**A**) Upper panel, immunohistochemical staining for β-catenin in different areas of the sham group hearts; Lower panel, immunohistochemical staining for β-catenin in different areas of the MI group hearts. (**B**) Upper panel, immunohistochemical staining for collagen-8 in different areas of the sham group hearts; Lower panel, immunohistochemical staining for collagen-8 in different areas of the MI group hearts. Left: infarct area; Middle: border area; Right: remote area.

Supplementary Tables

Supplementary Table 1. The 86 genes in the green module of the WGCNA analysis

ENSMUSG00000000776	Polr3d
ENSMUSG00000001774	Chordc1
ENSMUSG00000002981	Clptm1
ENSMUSG00000005483	Dnajb1
ENSMUSG00000007617	Homer1
ENSMUSG00000007721	Ccdc124
ENSMUSG00000007777	0610009B22Rik
ENSMUSG00000007877	Tcap
ENSMUSG00000008668	Rps18
ENSMUSG00000013878	Rnf170
ENSMUSG00000014226	Cacybp
ENSMUSG00000014294	Ndufa2
ENSMUSG00000018906	P4ha2
ENSMUSG00000020092	Pald1
ENSMUSG00000020482	Ccdc117
ENSMUSG00000020827	Mink1
ENSMUSG00000021361	Tmem14c
ENSMUSG00000022237	Ankrd33b
ENSMUSG00000022426	Josd1
ENSMUSG00000022433	Csnk1e
ENSMUSG00000024219	Anks1
ENSMUSG00000024247	Pkdcc
ENSMUSG00000024900	Cpt1a
ENSMUSG00000024966	Stip1
ENSMUSG00000024978	Gpam
ENSMUSG00000025261	Huwe1
ENSMUSG00000025558	Dock9
ENSMUSG00000025907	Rb1cc1
ENSMUSG00000026500	Cox20
ENSMUSG00000026977	07-Mar
ENSMUSG00000027255	Arfgap2
ENSMUSG00000028034	Fubp1
ENSMUSG00000028271	Gtf2b
ENSMUSG00000028318	Polr1e
ENSMUSG00000028427	Aqp7
ENSMUSG00000030653	Gm45837
ENSMUSG00000031068	Glrx3
ENSMUSG00000031167	Rbm3
ENSMUSG00000031309	Rps6ka3
ENSMUSG00000031667	Aktip
ENSMUSG00000032295	Man2c1
ENSMUSG00000032942	Ucp3

ENSMUSG00000033020	Polr2f
ENSMUSG00000033191	Tie1
ENSMUSG00000035242	Oaz1
ENSMUSG00000035849	Krt222
ENSMUSG00000036585	Fgf1
ENSMUSG00000037266	Rsrp1
ENSMUSG00000037805	Rpl10a
ENSMUSG00000038550	Ciart
ENSMUSG00000038880	Mrps34
ENSMUSG00000040026	Saa3
ENSMUSG00000040269	Mrps28
ENSMUSG00000040459	Arglu1
ENSMUSG00000046691	Chtf8
ENSMUSG00000048007	Timm8a1
ENSMUSG00000052305	Hbb-bs
ENSMUSG00000054364	Rhob
ENSMUSG00000055116	Arntl
ENSMUSG00000056749	Nfil3
ENSMUSG00000057580	Gm10012
ENSMUSG00000058135	Gstm1
ENSMUSG00000059824	Dbp
ENSMUSG00000060147	Serpinb6a
ENSMUSG00000060152	Pop5
ENSMUSG00000063077	Kif1b
ENSMUSG00000064326	Siva1
ENSMUSG00000064791	Snord14e
ENSMUSG00000064796	Terc
ENSMUSG00000067547	Gm7666
ENSMUSG00000067847	Romo1
ENSMUSG00000069917	Hba-a2
ENSMUSG00000069919	Hba-a1
ENSMUSG00000070803	Cited4
ENSMUSG00000071347	C1qtnf9
ENSMUSG00000071540	3425401B19Rik
ENSMUSG00000072772	Grcc10
ENSMUSG00000073940	Hbb-bt
ENSMUSG00000076128	Mir686
ENSMUSG00000078915	Hsp25-ps1
ENSMUSG00000091562	Crybg3
ENSMUSG00000097656	Gm26712
ENSMUSG00000098462	Gm27694
ENSMUSG00000106362	AL672049.1
ENSMUSG00000107283	Mpv17
ENSMUSG00000107478	Gm45234

Supplementary Table 2. GSEA report for upregulated pathways

NAME	SIZE	ES	NES	NOM *p*-val	FDR *q*-val	FWER *p*-val	LEADING EDGE
PANTHER_MM_INTEGRIN_SIGNALLING_PATHWAY	54	0.605	2.231	0.000	0.000	0.000	tags=59%, list=22%, signal=75%
INOH_MM_INTEGRIN	35	0.665	2.190	0.000	0.000	0.000	tags=69%, list=23%, signal=88%
WIKIPATHWAYS_MM_FOCAL_ADHESION-WP306	54	0.592	2.162	0.000	0.000	0.000	tags=57%, list=22%, signal=72%
PANTHER_MM_CYTOSKELETAL_REGULATION_BY_RHO_GTPASE	26	0.636	1.983	0.000	0.002	0.011	tags=73%, list=27%, signal=100%
NETPATH_MM_EGFR1_SIGNALING_PATHWAY	136	0.426	1.826	0.000	0.019	0.108	tags=46%, list=27%, signal=61%
WIKIPATHWAYS_MM_REGULATION_OF_ACTIN_CYTOSKELETON-WP51	37	0.533	1.776	0.001	0.028	0.182	tags=62%, list=27%, signal=84%
NETPATH_MM_WNT_SIGNALING_PATHWAY	21	0.570	1.681	0.018	0.066	0.421	tags=48%, list=21%, signal=60%
PANTHER_MM_HUNTINGTON_DISEASE	43	0.472	1.653	0.006	0.078	0.529	tags=77%, list=40%, signal=126%
PANTHER_MM_ALZHEIMER_DISEASE-PRESENILIN_PATHWAY	16	0.611	1.651	0.014	0.071	0.534	tags=44%, list=8%, signal=47%

Supplementary Table 3. GSEA report for downregulated pathways

NAME	SIZE	ES	NES	NOM *p*-val	FDR *q*-val	FWER *p*-val	LEADING EDGE
WIKIPATHWAYS_MM_ELECTRON_TRANSPORT_CHAIN-WP111	64.000	–0.751	–3.185	0.000	0.000	0.000	tags=86%, list=20%, signal=105%
WIKIPATHWAYS_MM_OXIDATIVE_PHOSPHORYLATION-WP623	36.000	–0.764	–2.854	0.000	0.000	0.000	tags=81%, list=14%, signal=93%
INOH_MM_CITRATE_CYCLE	21.000	–0.716	–2.302	0.000	0.000	0.000	tags=76%, list=20%, signal=94%
WIKIPATHWAYS_MM_FATTY_ACID_BETA_OXIDATION-WP143	21.000	–0.706	–2.243	0.000	0.000	0.000	tags=67%, list=19%, signal=82%
WIKIPATHWAYS_MM_TCA_CYCLE-WP78	29.000	–0.627	–2.184	0.000	0.000	0.001	tags=69%, list=20%, signal=85%
WIKIPATHWAYS_MM_GLYCOLYSIS_AND_GLUCONEOGENESIS-WP534	27.000	–0.617	–2.156	0.000	0.000	0.002	tags=63%, list=21%, signal=79%

Supplementary Table 4. Gene alteration in WNT signaling pathway

PROBE	RANK IN GENE LIST	RANK METRIC SCORE	RUNNING ES
SFRP2	26	1.233115	0.151679
LRP1	188	0.748588	0.200758
KREMEN1	258	0.660285	0.265666
CTNNB1	266	0.650148	0.347624
YWHAB	400	0.535507	0.377453
CCND1	469	0.498205	0.42171
RHOA	494	0.479338	0.476556
ILK	519	0.463446	0.529349
AKT1	686	0.395137	0.531264
RAC1	724	0.381176	0.569574
CSNK1A1	1033	0.273293	0.513692
CDH2	1216	0.211877	0.487182
PPP2CA	1388	0.158804	0.457071
MAPK1	1410	0.15206	0.470506
RYK	1478	0.129619	0.467419
JUP	1635	0.085088	0.432221
CTBP1	1651	0.08129	0.438286
PRKACA	2156	–0.07241	0.2984
PPP1CA	2285	–0.10943	0.27464
JUN	2440	–0.15866	0.249543
RAF1	2683	–0.25956	0.21143

Supplementary Table 5. Gene alterations in integrin signaling pathway

PROBE	RANK IN GENE LIST	RANK METRIC SCORE	RUNNING ES
COL8A1	24	1.250044	0.041699
ITGBL1	34	1.204578	0.086106
COL4A2	46	1.108793	0.126169
ITGB5	51	1.086318	0.167447
COL5A2	128	0.846045	0.1778
COL4A1	129	0.839928	0.21064
COL6A2	131	0.83876	0.243136
COL6A1	132	0.838017	0.275902
ACTN4	141	0.824349	0.305741
RHOB	157	0.788537	0.332087
FN1	159	0.787086	0.362562
COL3A1	190	0.747269	0.382808
RHOC	213	0.717562	0.404286
LAMC1	314	0.605321	0.398049
FLNA	321	0.59947	0.419694
CAV1	363	0.55932	0.429302
RAP1B	389	0.540683	0.442966
ITGB1	425	0.525241	0.453036
ARPC1A	441	0.514583	0.46867
COL1A2	453	0.507689	0.485231

CDC42	459	0.505299	0.503493
RHOA	494	0.479338	0.512067
ILK	519	0.463446	0.52301
TLN1	521	0.462268	0.540786
LAMA4	542	0.455688	0.552622
ARPC1B	594	0.432813	0.554293
ARPC5	623	0.421344	0.562394
ARF6	631	0.418681	0.576671
LAMB2	669	0.401626	0.58131
RRAS	681	0.396598	0.593527
RAC1	724	0.381176	0.595871
ACTB	742	0.376136	0.605494
ARPC3	871	0.327444	0.580019
MAP3K3	883	0.324298	0.58941
ARPC2	934	0.305842	0.586416
VCL	1071	0.260906	0.555947
ARL1	1082	0.256929	0.563002
ARF1	1207	0.213645	0.534274
MAP2K1	1262	0.198721	0.525896
CRK	1363	0.166898	0.502517
MAPK1	1410	0.15206	0.494707
ACTG1	1494	0.125848	0.474807
ACTN2	1513	0.122105	0.474198
LIMS1	1678	0.071031	0.427932
RAP1A	1680	0.0706	0.430394
LAMB1	1707	0.063852	0.425115
MAP2K2	2045	–0.0357	0.325733
LIMS2	2364	–0.13732	0.236007
ITGA7	2570	–0.21246	0.18301
RAF1	2683	–0.25956	0.159666
ARHGAP10	2686	–0.26164	0.169298
ARAF	2689	–0.26324	0.178992
PIK3R1	2831	–0.32677	0.149604
GRB2	3099	–0.49504	0.089115

Supplementary Table 6. Gene alterations in fatty acid beta oxidation pathway

PROBE	RANK IN GENE LIST	RANK METRIC SCORE	RUNNING ES
HADH	1575	0.105087	–0.45296
TPI1	2110	–0.05695	–0.60381
PNPLA2	2190	–0.0827	–0.61663
CHKB	2217	–0.09075	–0.61273
ACAT1	2221	–0.0911	–0.60197
ACSL1	2484	–0.17422	–0.65729
CPT1B	2599	–0.22258	–0.66259
DLD	2746	–0.29057	–0.66868
ACADL	2764	–0.29748	–0.63569
LPL	2801	–0.31471	–0.60612

ACADS	2830	–0.32602	–0.57274
CPT2	2932	–0.38384	–0.55359
ACADM	3000	–0.4278	–0.51874
GCDH	3038	–0.45053	–0.47211
DECR1	3070	–0.4718	–0.42098
HADHA	3173	–0.55233	–0.38058
SLC25A20	3197	–0.57364	–0.31407
CRAT	3199	–0.58078	–0.24013
ECHS1	3263	–0.67054	–0.17307
ACADVL	3276	–0.68272	–0.08935
ECI1	3351	–0.97703	0.013621

Supplementary Table 7. Gene alterations in glycolysis and gluconeogenesis pathway

PROBE	RANK IN GENE LIST	RANK METRIC SCORE	RUNNING ES
PFKP	744	0.375565	–0.17815
HK1	842	0.339539	–0.16844
PFKL	1186	0.221405	–0.2451
GPI1	1476	0.130336	–0.31606
PGK1	1863	0.017227	–0.42862
TPI1	2110	–0.05695	–0.49514
PGAM1	2240	–0.09476	–0.52267
PKM	2281	–0.10786	–0.52231
PDHX	2291	–0.11455	–0.512
DLAT	2333	–0.12668	–0.5098
PFKM	2696	–0.26618	–0.58703
PGAM2	2704	–0.27234	–0.55824
HK2	2712	–0.27505	–0.52915
LDHA	2719	–0.27801	–0.49942
MDH2	2744	–0.29021	–0.47365
DLD	2746	–0.29057	–0.44102
PDHA1	2846	–0.3355	–0.43237
MDH1	2868	–0.35118	–0.3988
GOT2	3013	–0.4349	–0.39223
SLC2A4	3030	–0.4472	–0.3463
PDHB	3051	–0.45979	–0.30013
ALDOA	3116	–0.50893	–0.26144
ENO3	3147	–0.53595	–0.20961
LDHB	3201	–0.58166	–0.15941
ATP5G1	3220	–0.60351	–0.09636
GM10039	3224	–0.60566	–0.02861
GOT1	3286	–0.70273	0.032928

Supplementary Table 8. Gene alterations in TCA cycle pathway

PROBE	RANK IN GENE LIST	RANK METRIC SCORE	RUNNING ES
PDK4	431	0.518681	–0.07767
PDP1	899	0.318727	–0.1854
OGDH	1073	0.260313	–0.21152
IDH2	1230	0.209108	–0.23756
SUCLG2	2185	–0.08099	–0.51288
DLST	2266	–0.1051	–0.52644
PDK1	2288	–0.11027	–0.52199
PDHX	2291	–0.11455	–0.51148
DLAT	2333	–0.12668	–0.51138
SDHD	2725	–0.28036	–0.60027
MDH2	2744	–0.29021	–0.57748
DLD	2746	–0.29057	–0.54962
IDH3G	2754	–0.29351	–0.52326
PDHA1	2846	–0.3355	–0.51776
MDH1	2868	–0.35118	–0.48996
ACO2	2907	–0.37008	–0.46537
SDHC	2914	–0.37358	–0.43095
IDH3A	2931	–0.38174	–0.3987
SDHB	3022	–0.44	–0.38278
SUCLA2	3023	–0.44078	–0.34006
CS	3027	–0.4455	–0.29778
IDH3B	3028	–0.44555	–0.2546
PDK2	3041	–0.45338	–0.21423
PDHB	3051	–0.45979	–0.17234
FH1	3081	–0.47873	–0.13456
SDHA	3150	–0.53694	–0.10271
SUCLG1	3214	–0.59806	–0.06345
ATP5G1	3220	–0.60351	–0.00645
GM10039	3224	–0.60566	0.05135

Supplementary Table 9. Ninety five genes simultaneously differentially regulated at both 1 and 8 months after MI

gene	baseMean	baseMean	log2FC_1m	log2FC_8m	padj_1m	padj_8m
9330159F19Rik	72.38382	263.2386	1.338094853	0.772947365	0.017056744	0.013809142
Abca12	469.6926	907.8357	–1.58722346	–1.243272159	3.36E-10	0.000107469
AC022682.2	61.96831	80.27954	–1.994359763	–1.33919269	2.14E-05	0.039376723
AC157516.1	69.37918	179.0611	–2.157162233	–1.636440248	9.17E-06	0.002207262
Adamts20	33.94426	91.08125	1.77092724	1.660193472	0.00091548	3.46E-06
Adamtsl1	165.3911	496.4326	1.451609157	0.537405511	1.54E-07	0.022820712
Adcy8	27.36026	51.14039	–1.622768953	–1.993648065	0.007910621	3.46E-06
Add2	32.75743	39.58893	2.425409933	1.206885392	0.000488474	0.001304079
AL591207.3	17.84717	28.20068	3.507431259	1.499062707	0.000266199	0.02008895
Aldh1l2	338.0175	670.2361	–1.325518758	–0.744502034	8.32E-07	0.028921143
Ankrd63	33.96433	107.6297	–2.036353914	–1.157061168	6.31E-05	0.028436322
Aqp2	20.00909	44.6289	1.914123072	1.709417141	0.015780422	0.004250746
Atp8b4	89.5417	406.8387	1.814641735	–0.657079691	2.93E-08	0.049443001
Azin2	89.13142	209.8742	0.984562372	0.935053131	0.006373882	2.94E-07
B4galnt3	31.85274	75.94876	8.307744623	2.056435946	2.89E-08	1.54E-07
Btla	61.95872	128.2981	0.900534149	1.446972316	0.01685731	6.03E-06
Carmil3	84.0663	146.8175	–1.237885337	–0.736173573	0.004326839	0.007285041
Ccdc88b	102.5025	347.5408	0.963590651	–0.587584473	0.017493028	0.042258024
Ccnj	300.905	602.3457	–0.686261923	–0.381715554	0.000265836	0.022820712
Cd22	24.32314	59.99578	2.062886595	2.350666596	0.002042038	8.27E-07
Cdh3	19.31972	73.22186	7.587282833	1.05376394	3.70E-07	0.011799969
Cenpe	100.7449	246.5119	1.235381018	–0.838841904	0.00786079	0.008075965
Clec18a	42.49937	64.59779	–2.194397745	–1.259674449	0.000188506	0.009800352
Col11a1	150.3847	192.7107	5.530428761	1.319914559	1.78E-09	0.046809408
Col27a1	355.7013	443.4263	0.940474882	0.430679306	0.000897193	0.023879553
Crb1	47.02913	83.74538	–2.044517118	–1.229102818	0.000852805	0.012802213
Csf2rb2	57.18061	179.2012	2.032208005	1.050353439	1.25E-05	0.020314203
Dchs2	190.7537	267.483	3.014351889	1.556945263	9.63E-22	1.12E-06
Ereg	42.28248	116.9084	5.215061922	1.724405437	1.09E-09	1.41E-05
Esr1	75.94608	297.3961	1.41602485	0.764006532	0.003032061	0.047435928
Exoc3l2	59.00953	252.4834	1.083413536	0.730190962	0.008056726	0.008757768
Eya4	88.7854	157.3741	2.052361136	1.067523645	3.76E-06	0.008094616
Faim2	15.37698	87.69929	4.430092583	2.564079235	0.000253018	4.64E-08
Fam171b	119.2217	269.3606	1.146632937	0.709317266	0.004534949	0.000717559
Flt3	16.80729	54.71801	4.447239656	1.473136516	0.000609507	0.002537139
Fmn1	116.176	268.8948	1.599808852	1.346818513	1.48E-05	0.002798257
Gabrb3	21.80811	49.84956	2.087083127	1.684009619	0.002830015	0.002798257
Gabrr2	45.87044	68.02024	–1.866615384	–1.519079251	0.00026071	0.001018617
Gcnt4	45.7202	57.86883	2.894881795	1.358232514	5.21E-09	0.047670774
Gli2	85.43764	131.6428	1.820966739	0.679523708	1.43E-05	0.002270175
Gng8	43.2071	59.78843	3.703775196	2.125041857	6.28E-08	1.47E-05
Gprin3	79.06171	177.0166	0.982998678	1.286644524	0.026854629	0.002537139
Greb1	57.37384	57.11321	1.588753271	0.953314325	0.0055535	0.011017089
Gria3	193.0349	250.5424	1.905922134	0.805614693	1.30E-10	0.013596458
H2-Ob	46.0266	106.5466	1.145888193	1.039805101	0.01422812	0.009800352
Hebp2	48.05972	139.9614	2.209293862	0.740453665	4.19E-07	0.001097243
Hephl1	16.70996	48.75719	4.986008608	2.555201241	0.000360475	0.002237368
Hgf	95.50513	333.1287	1.023382578	0.613775256	0.014562949	1.76E-05

Il1rl2	173.3036	310.0596	0.738374965	0.762135194	0.025622396	0.032075891
Il6	24.57122	44.46563	3.580218916	2.015820222	1.59E-05	0.022246819
Kcna6	58.95865	148.0705	–1.690368067	–1.033712286	0.000326346	0.021063736
Kcnj14	49.22876	78.13598	1.106644663	1.423185549	0.0416764	0.000191724
Kif2c	16.6513	76.90939	2.289965649	–0.883948709	0.017160253	0.047670774
Kif6	109.24	196.2545	–1.022273418	–0.670650265	0.004250182	0.009567669
Klhl29	97.04787	144.4202	2.319237182	1.323077437	1.10E-12	8.27E-07
Lgi3	108.5846	196.035	–1.168515181	–1.149833657	0.001143076	0.000839157
Lrp8	52.63052	68.47234	2.17990467	1.688064528	2.89E-05	0.000705942
Mgat5b	21.88977	74.99011	3.284347677	1.681484684	0.000217058	0.014531136
Mmp12	29.26492	186.795	1.442865736	1.614741137	0.009105975	0.004494978
Mylk2	19.4292	23.98107	7.597182009	1.356109249	7.64E-07	0.01630661
Osgin1	70.18034	163.4612	–0.848248138	–0.766289406	0.045968856	0.038826495
P2ry10	25.68545	109.2988	1.507248036	1.3779083	0.02045988	0.000839157
P4ha3	26.37245	35.69365	8.037336988	2.220418479	2.24E-08	0.006814691
Padi4	28.44141	62.34945	1.469349664	1.206210285	0.027370478	0.008492938
Pak3	81.95312	166.8805	2.832568299	2.024932516	3.36E-10	7.13E-06
Pira2	17.9124	217.0514	3.275330959	–1.325123732	0.010418457	3.91E-05
Pitpnm3	122.0296	145.7451	–1.213835066	–0.642499843	6.31E-05	0.022820712
Rab17	50.76643	89.00408	–1.245182676	–1.058803418	0.00547896	0.007285041
Rasgef1a	37.1663	150.3048	1.412350672	1.577620716	0.004241616	1.36E-05
Rassf10	116.5135	245.6662	–0.585507308	0.525495859	0.043312449	0.049865687
Ret	212.9693	506.869	–1.404154551	–1.082278928	9.69E-10	3.10E-05
RMST_1	92.13399	161.2933	–1.081845815	–0.913073663	0.01617561	0.00097616
Scg2	33.79235	56.83588	8.395686327	4.52288006	3.61E-09	2.83E-13
Sec16b	270.5756	403.384	1.297867542	0.647384726	1.94E-10	0.001215566
Slc6a7	51.69015	41.8191	5.803694687	2.310969091	1.71E-12	0.001225144
Slit2	636.5364	1174.787	0.895635384	0.534440627	2.22E-05	1.71E-06
Sntg2	40.96716	119.7424	8.672300191	2.121286353	4.42E-10	5.02E-09
Specc1	290.5399	501.3615	0.598185465	0.459398396	0.011156035	0.000839157
Sphk1	59.47501	191.2715	1.368656126	0.89744868	0.002773203	0.001185865
Srgap3	131.9378	175.2212	2.65425815	0.822610595	3.61E-09	0.004971559
St14	35.53093	88.13187	3.92784732	1.01547955	7.49E-10	0.009497068
Steap2	119.16	258.9819	1.726286203	0.888052602	2.57E-08	0.001723239
Tbx15	49.93634	140.4692	1.104645046	1.524652685	0.015516497	0.000139045
Tc2n	46.51239	133.5308	2.431350799	0.823009946	2.12E-06	0.009369206
Tmem56	147.233	562.4513	–1.209475891	–1.009392798	0.000664798	3.46E-06
Tmprss13	39.14196	149.0266	–1.575697533	–1.033357272	0.00147481	0.044786353
Tnni2	28.0641	68.64875	–1.14286515	–0.915060635	0.03912346	0.004258662
Trpm6	47.30285	99.68346	2.001789475	1.131149033	3.13E-05	0.000705942
Wscd2	40.32155	83.34609	3.789955949	1.548127677	4.50E-07	0.002942176
Xylt1	244.5109	426.3965	1.122938768	0.540895006	2.19E-06	0.001160318
Zfp30	425.8207	634.8073	–0.752838829	–0.53850983	9.80E-06	0.008757768
Zfp354c	275.2212	512.1063	0.888658091	0.638990311	1.48E-06	0.001798011
Zfp423	154.85	365.9361	1.532558639	0.547260101	7.06E-08	0.001086937
Zfp783	80.43104	135.5416	1.066661879	0.809561367	0.002956994	0.002038413
Zfp995	85.12412	168.2397	0.868114571	0.684070644	0.041180192	0.002653893

Supplementary Video

Supplementary Video 1. Shortness of breath in a mouse with decompensated heart failure observed at 8 months after MI.

Supplementary Raw Data

Supplementary Raw Data. Supplementary raw data of all gene count matrix and differentially expressed genes at 1 and 8 months after MI.

Please browse Full Text version to see the Supplementary video and raw data.